Thermal focusing and optical bistability in ferroelectrics

2001 J. Phys.: Condens. Matter 13 R195

(http://iopscience.iop.org/0953-8984/13/12/202)

INSTITUTE OF PHYSICS PUBLISHING JOURNAL OF PHYSICS: CONDENSED MATTER

J. Phys.: Condens. Matter **13** (2001) R195–R234 www.iop.org/Journals/cm PII: S0953-8984(01)16724-X

TOPICAL REVIEW

Thermal focusing and optical bistability in ferroelectrics

R A O'Sullivan[1,2], K W McGregor[1] and J F Scott[2]

[1] Department of Applied Physics, Royal Melbourne Institute of Technology, GPO Box 2476V, Melbourne, Victoria 3001, Australia
[2] Department of Earth Sciences, University of Cambridge, Cambridge CB2 3EQ, UK

Received 31 August 2000, in final form 7 December 2000

Abstract

A review is presented of phenomena involving thermal focusing and optical bistability arising from the temperature dependence of the refractive index in ferroelectrics. Aperiodic spatio-temporal oscillations have been observed in the light transmitted and reflected by parallel-sided crystal and ceramic samples of the thermo-optic ferroelectrics PMN (lead magnesium niobate, $Pb(Mg_{1/3}Nb_{2/3})O_3$), PLZT (lanthanum doped lead zirconium titanate, $Pb(Zr_{1-x}Ti_x)O_3$:La), BNN (barium sodium niobate, $Ba_2NaNb_5O_{15}$) and Ce:SBN (cerium doped strontium barium niobate, Ce^{3+}:$Sr_xBa_{1-x}Nb_2O_6$) under steady illumination by an incident c.w. laser beam of finite beamwidth. Such materials focus the incident beam due to the temperature dependence of the refractive index and the establishment of a radial temperature gradient. The shape of the resulting thermal lens varies in time as a result of variation in the absorbed energy arising from both thermal focusing and optical bistability (Fabry–Pérot resonance). Whereas PMN and PLZT exhibit relaxation oscillations, the beam oscillations produced by BNN and Ce:SBN have equal rise and fall times. We compare the predictions of theoretical models with experimental results for ferroelectric ceramics and crystals. The principal conclusions from the present work are that (1) there are two distinct mechanisms for aperiodic oscillation in dispersively nonlinear plates, *viz*., focusing oscillations and Fabry–Pérot switching oscillations, of which only the latter involves bistability; (2) in Fabry–Pérot etalons with a diffusive nonlinearity, as contrasted with the systems (e.g. laser tubes) originally described by Gordon *et al*, the diffusive quantity (i.e. temperature) can exhibit bistable and multistable switching behaviour, leading to regenerative oscillations in other variables (e.g. light output); (3) there are two characteristic relaxation times involved in these oscillations, differing by several orders of magnitude; (4) the spatio-temporal characteristics of the transmitted beam patterns in the near and far fields can be quantitatively predicted and (5) comparison between theory and experiment can provide information on the temperature dependence of conductivity and thermo-optic coefficient near the ferroelectric phase transition.

Glossary of symbols used

$A(u, \zeta, \tau)$	absorption factor
A_s	constant smoothed absorption factor
A_{max}	maximum absorption factor
A_{min}	minimum absorption factor
B_n	coefficient in Green function (appendix A)
C_n	coefficient in Green function (appendix A)
C	$C = A_s P/4\pi LK$ (appendix B)
D_n	coefficient in Green function (appendix A)
$E(u, \zeta)$	light field within Fabry–Pérot resonator
$E_F(r, z)$	light field of the forward travelling wave
$E_B(r, z)$	light field of the backward travelling wave
$E_0(u, \zeta)$	slowly varying wave amplitude
$E_1(x)$	exponential integral function: $\int^{\infty} \mathrm{d}t\, \mathrm{e}^{-t}/t$
F_α	coefficient of finesse: $F_\alpha = 4R\,\mathrm{e}^{-\alpha L}/(1 - R\,\mathrm{e}^{-\alpha L})^2$
$\mathcal{F}$	Fresnel number $= L/kn_0w_0^2$
$G(u, \zeta, \theta, \tau; u', \zeta', \theta', \tau')$	Green function (appendix A)
$G(s, \tau)$	Hankel transform: $G(s, \tau) = \int_0^{\infty} \mathrm{d}u\, u J_0(su) \exp(-2u^2) A(u, \tau)$
G	$G = A_s P(\mathrm{d}n/\mathrm{d}T)/\pi w^2 LKn_0$
H	linearized heat transfer coefficient
I_c	beam irradiance within the sample
I_i	incident beam irradiance $I_i(r) = I_p \exp(-2r^2/w^2)$
I_p	peak incident irradiance $I_p = 2P/\pi w^2$
I_0, I_1	modified Bessel function of the first kind of order 0, 1
J_0	Bessel function of order zero
K	thermal conductivity
K_0, K_1	modified Bessel function of the second kind of order 0, 1
L	sample thickness
M	number of thermal switches
$M\{\tau, \tau', T(0, \tau')\}$	kernel of the Volterra integral
P	incident light power $P = \pi w^2 I_p/2$
P_{abs}	absorbed power
P_T	transmitted power
Q	parameter $Q = 4k^2 n_0^2 w^4$
R	reflection coefficient
$S(u, \zeta)$	eikonal function
$T(r, z, t)$	temperature increment above ambient within sample
$\bar{T}(u, \tau)$	temperature above ambient averaged over sample thickness
$\tilde{T}(s, \tau)$	Hankel transform of temperature averaged over sample thickness
$T_{sm}(u, \tau)$	smoothed temperature profile
$\mathcal{T}$, $\mathcal{T}'$	amplitude transmission coefficient for light entering/leaving the sample
U	parameter $U^2 = u^2 + u'^2 - 2uu' \cos(\theta - \theta')$ (appendix A)

$U_\eta(u)$, $U_\sigma(u)$	functions of u (appendix B)
$V(g)$	'potential energy' function (appendix B)
W	parameter $W = -96L^2/k^2n_0^2w^4$ (appendix B)
$Z_\eta(\zeta)$, $Z_\sigma(\zeta)$	functions of ζ (appendix B)
b	sample radius
c	specific heat
c_0	speed of light in vacuum
e	base of natural logarithm (exp)
$f(\zeta)$	function: $2f^2(\varsigma) = 1 + (QG)^{-1} + [1 - (QG)^{-1}]\cos(2L\sqrt{G}\varsigma)$
$g(\zeta)$	ansatz function (Ein approximation) $\beta(\zeta) = -w^2g'(\varsigma)/8L^2$ (appendix B)
$g_n(\zeta)$	function $g_n(\varsigma) = (\eta_n \cos \eta_n\varsigma + h \sin \eta_n\varsigma)$ (appendix A)
h	parameter $h = HL/K$
k	free space wavenumber $k = 2\pi/\lambda$
m	integer index (mode number)
n	refractive index
$p(\zeta)$	function $p(\zeta) = \mathrm{e}^{-g(\zeta)} - 1$ (appendix B)
r	cylindrical polar coordinate
s	Hankel transform variable
t	time
t_K	conduction time $t_K = w^2\rho c/K$
t_c	convection–radiation relaxation time $t_c = \rho cL/2H$
u	reduced radius $u = r/w$
w	beamwidth
x	arbitrary variable
z	axial coordinate
α	extinction coefficient
α_a	absorption coefficient
α_s	scattering coefficient
β_m	roots of the characteristic equation: $\tan(\beta_m/2) = h/\beta_m$ (appendix A)
$\beta(\zeta)$	ansatz function
β, γ, δ	critical exponents (section 6)
γ'	Euler's constant = 0.577 21 ...
γ_n	roots of the characteristic equation: $\tan \gamma_n = 2\gamma_n h/(\gamma_n^2 - h^2)$ (appendix A)
δ_m	roots of the characteristic equation: $\tan(\delta_m/2) = -\delta_m/h$ (appendix A)
$\eta(u, \zeta)$, $\sigma(u, \zeta)$	transformed variables (appendix B)
ζ	reduced axial coordinate z/L
χ	parameter $\chi = (\mathrm{d}n/\mathrm{d}T)/n_0 + (\mathrm{d}L/\mathrm{d}T)/L$, $n(T) = n_0(1 + \chi T)$
κ	thermal diffusivity $\kappa = K/\rho c$
$\phi(\zeta)$	variable phase parameter
λ	free space wavelength
μ	parameter $\mu^2 = 2Hw^2/LK$
ν	variable of integration
ρ	density
θ	angular variable of integration
τ	reduced time $\tau = t/t_K$

1. Introduction

All transparent substances, including solids, liquids, and gases, display the thermo-optic effect, i.e. their refractive index n depends on temperature T. This temperature dependence of n produces two distinct experimental effects, which may occur separately or in combination, namely *thermal lensing*, either focusing or defocusing, which occurs when the incident beamwidth is small compared to the sample thickness, and *optical bistability*, which occurs in the presence of a feedback mechanism.

Thermal lensing was originally studied by Gordon, Leite *et al* at Bell Labs in the early 1960s because it produces defocusing in gas lasers, which was regarded as a nuisance. In gases, thermal lensing always involves defocusing, because the refractive index $n(T)$ is proportional to the density of the gas, which necessarily decreases with increasing temperature; thus $\mathrm{d}n/\mathrm{d}T$ is negative, with the focal strength proportional to $\mathrm{d}n/\mathrm{d}T$.

Thermal focusing was first observed in solids in the crystalline ferroelectric lithium niobate ($LiNbO_3$) by Akhmanov *et al* (1967, 1968a, b) and in ferroelectric ceramics by Altshuler *et al* (1986). In crystals $n(T)$ can either increase or decrease with temperature. As phase transition temperatures T_c are approached from below, it is usual that one index increases sharply and another decreases. For example, in a tetragonal–cubic transition, two indices become equal at the transition temperature but one increases below T_c and the other decreases. For a continuous phase transition the derivative $\mathrm{d}n/\mathrm{d}T$ actually diverges at T_c. Since the thermal focal strength is proportional to $\mathrm{d}n/\mathrm{d}T$, this produces extremely large focusing effects very near T_c. For this reason thermal lensing is best studied near continuous (second order or tricritical) phase transition points. Indeed, accurate information about the critical exponents beta, characterizing the order parameter, and delta, characterizing the isothermal response to conjugate fields, can be obtained.

As pointed out by Gibbs (1985), optical bistability cannot be produced by thermo-optic nonlinearity alone; it requires feedback, e.g. in a Fabry–Pérot or ring cavity. For parallel-sided, polished samples of appropriate thickness, the absorption coefficient and reflectivity of some materials is such that they constitute *intrinsic* Fabry–Pérot resonators. In combination with the thermo-optic effect this feedback mechanism can give rise to photo-thermal optical bistability, which has important device applications. It was first recognized by Grohs *et al* (1990) that photo-thermal optical bistability could be used as a photonic temperature sensor. Although this is truly photonic (no wires in or out), it is relatively slow (ms) and hence not in the family of ultrafast (fs) photonic devices. Nevertheless, it can be of real utility in remote sensing in hazardous environments. Other applications, to be discussed below, include gas flow sensors (the effect in crystals is sensitive to convection at the sample surfaces), negative feedback intra-cavity noise limiters for lasers, and related practical devices.

One of the surprises encountered in experiments on ferroelectrics was that they exhibit oscillatory output, either with or without optical bistability (including regenerative pulsations) even in the absence of *external* feedback. This is because only certain ferroelectric samples have appropriate values of absorption coefficient and reflectivity to constitute *intrinsic* Fabry–Pérot resonators for a given sample thickness. Since such samples simultaneously exhibit thermal focusing and bistability, their effect on focused laser beams can be described neither by simple thermal focusing theory based on an equation first-order in time (which does not permit oscillatory solutions) nor by the theory of longitudinal (plane wave) optical bistability. In fact the rigorous theory provided in the present review shows that oscillation can be expected under a broad range of realistic parameters and at very low powers ($<$100 mW). Thus this thermo-optic bistability is not in the usual high-power regime of nonlinear optics, but can be realized with ordinary, inexpensive c.w. gas lasers (argon or helium–neon), making the

experiments accessible to a wide range of researchers. A second surprise afforded by careful analysis is that there are not one but two characteristic times in the problem, which differ by a factor of more than 1000. Thus, the perspective we now have on thermal focusing is radically different than in the 1970s. Most important is that this technique is cheap, easy and accurate, but as yet has been unexploited as a probe of condensed matter physics. The purpose of the present review is to provide condensed matter physicists with a comprehensive review of a useful new optical tool.

Optical bistability (OB) is defined by the existence of two discrete values of the optical output of a system for a single value of the input, over some range of the input power. OB has been extensively studied in a variety of systems, both experimentally and theoretically (Gibbs 1985). It may involve variation in the refractive index (*dispersive* OB) or the absorption coefficient (*absorptive* OB) of the sample. Initially, theoretical models were developed for *non-diffusive* OB in which the refractive index (Wagner *et al* 1968, Felber and Marburger 1976, Gagnon 1990) or absorption coefficient (Scott 1975, Scott *et al* 1975, see also the review by Scott 1986) depends directly on the *optical irradiance*. In these cases the system can be modelled in general by a pair of coupled nonlinear partial differential equations for the fields of the forward and backward travelling waves. Various techniques have been used to obtain solutions to these equations under a wide range of assumptions. Hybrid optical bistability (using an electrical delay line in the feedback) was reported in ceramic PLZT by Gibbs (1981). It was shown theoretically (Ikeda 1979, Ikeda *et al* 1980) and experimentally in atomic vapours and glass fibres (Nakatsuka *et al* 1983, Harrison *et al* 1983, 1984) that feedback in a ring cavity with an intensity-dependent refractive index (Kerr-type nonlinearity) can produce intrinsic non-diffusive optical bistability with regenerative pulsations, including period doubling. Models for non-diffusive *longitudinal* OB assuming incident plane waves were also developed for Fabry–Pérot feedback by Miller (1981), Jewell *et al* (1982), Wherrett (1984) and Garmire (1989) and for *transverse* OB involving incident beams of finite extent (Marburger and Felber 1978, Rozanov and Semenov 1980, Moloney and Gibbs 1982, Khoo *et al* 1984, Weaire *et al* 1985, Weaire and Kermode 1986, Vitrant *et al* 1990a, b, Reinisch and Vitrant 1990, see also the review by Abraham and Firth 1990).

Such models are inadequate to describe the *diffusive* nonlinearities which occur in ferroelectrics, including both thermal and photo-refractive effects (Rozanov 1981, Kurtz *et al* 1987, Seglins *et al* 1987, 1988, Krumins *et al* 1988). Spontaneous aperiodic oscillations in the intensity and spatial structure of the output beams have been observed under steady laser illumination of ferroelectrics such as PMN, PLZT, Ce:SBN and BNN (Chen *et al* 1992, Chen and Scott 1993a, b, Scott and Chen 1992) in which thermal focusing had been studied in detail (Scott *et al* 1990). Typical far field thermally focused beam patterns are shown in figure 1. In PMN the oscillations are smooth, i.e. they have approximately equal rise and fall times at low power (below about 0.1 W depending on sample thickness) but take the form of asymmetric relaxation oscillations at higher power (O'Sullivan *et al* 1996a), e.g. see figure 2. Initial observations with PLZT also showed smooth oscillations (Krumins *et al* 1995) but we have recently observed the transition from smooth oscillations to relaxation oscillations at an incident power of about 0.7 W in a 1 mm ceramic PLZT sample. In BNN and Ce:SBN, on the other hand, only smooth oscillations have been observed, e.g. figure 3. The reason for the absence of optical bistability and relaxation oscillations in BNN and Ce:SBN is different in each case and is discussed in section 3 of this paper. In the PMN and PLZT experiments, the Fabry–Pérot cavity formed by the parallel-sided sample is decoupled from the laser, either by a using a non-zero incidence angle or by interposing a quarter wave plate between the laser and the sample. Hence the observed oscillations are quite distinct from the oscillations between the longitudinal modes of a laser coupled to a Fabry–Pérot cavity discussed in the standard text

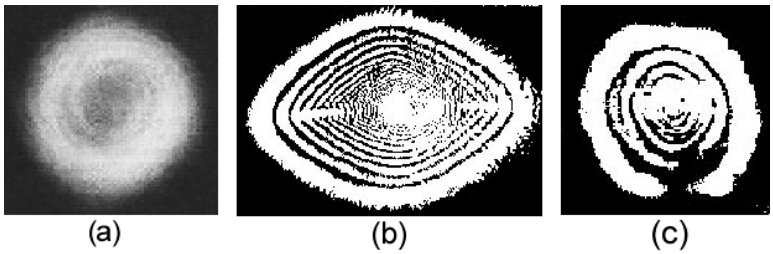

Figure 1. (a) Far field transmitted beam patterns from ceramic PMN plate under focused laser illumination (Chen and Scott 1993b). (b) Transmitted beam pattern from BNN, showing extreme anisotropy near T_C (Chen and Scott 1993a). (c) Transmitted beam pattern from SBN (Chen *et al* 1991b).

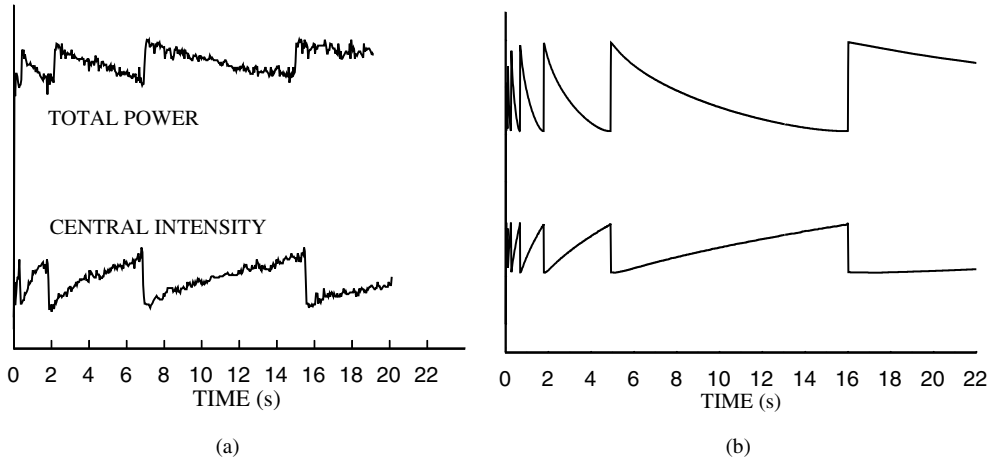

Figure 2. (a) Experimental central intensity, I_c, and total power transmitted by 0.74 mm thick PMN single crystal after step input at 514 nm, power 290 mW. (b) Computed transmitted power (top trace) and central transmitted intensity through PMN for same parameters as in (a) using equation (3.12) to calculate the temperature profile.

on laser physics (Sargent *et al* 1974) in terms of the Lotka–Volterra equations (Lotka 1925, Volterra 1926, 1931), by Goldstone and Garmire (1981) and Borenstein and Lamb (1972) using the Duffing equation and by Benkert and Anderson (1991) using the May–Leonard equations (May and Leonard 1975).

In *diffusive* dispersive OB, the refractive index depends on some variable, such as temperature or charge carrier concentration, which itself obeys a diffusion equation. Hence a theoretical model requires three coupled partial differential equations rather than two. For narrow incident beams, dispersive OB is coupled to thermal focusing. Analytic temperature profiles due to thermal focusing of a Gaussian incident beam were first derived by Gordon *et al* (1965) and subsequently by Whinnery *et al* (1967) using a linear differential equation which was first order in time. Their model lacked feedback and hence did not exhibit the 'photo-thermal bistability' subsequently observed in solids (Gibbs *et al* 1981, Scalora and Haus 1989). Wright *et al* (1985) showed the importance of carrier diffusion on a Kerr type nonlinearity but also without feedback. Rozanov (1981) derived a steady state solution for a diffusive absorptive nonlinearity in a thin sample with only one transverse dimension. Firth *et al* (1985) first treated the transverse effects of carrier diffusion in a system with (Fabry–Pérot)

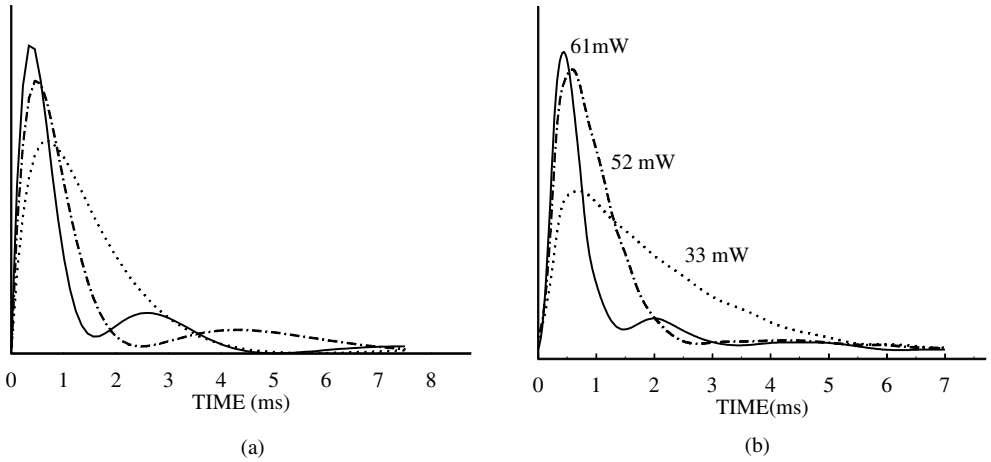

Figure 3. (a) Intensity decay at the centre of far field beam pattern transmitted by a 1.9 mm thick Ce^{3+}:$Sr_xBa_{1-x}Nb_2O_6$ (SBN) ceramic sample, using a 514 nm laser beam focused to a beamwidth of 190 μm (Chen *et al* 1991b). (b) Central intensity decay curves in SBN for the same parameters as in (a) resulting from the temperature profiles calculated using equation (3.1).

feedback provided by the boundary conditions on the forward and backward travelling light waves. Neglecting diffraction, dependence on the axial variable (z) and on one transverse dimension, they obtained numerical solutions for a 'top-hat' incident irradiance profile, i.e. $I_i(r)$ constant for $r < w$ and zero for $r > w$. Firth (1987) showed that this model, which corresponds to a hyperbolically driven oscillator, can lead to transverse symmetry breaking and chaos. Weaire and al-Hourani (1990) used a similar model neglecting diffraction to analyse the interaction among an incident set of delta function beams. Chen *et al* (1994) first modelled Fabry–Pérot feedback for an incident *Gaussian* beam in a thermo-optic material but assuming the temperature profile of Gordon *et al* (1965), instead of solving the coupled heat and field equations. An important step towards quantitatively matching the Fabry–Pérot etalon model to the number and timing of the experimentally observed relaxation oscillations in the focused laser beam transmitted by a ferroelectric sample was achieved by comparing the smoothed time-dependent radial temperature profile (given by the time-averaged Fabry–Pérot absorption factor) with the real time interferometrically measured temperature within a PMN crystal using an unfocused low power probe laser (O'Sullivan *et al* 1996b)—figure 4. In order to account quantitatively for both the longitudinal and transverse observed bistability phenomena in thermo-optic solids, however, it is necessary to solve the heat equation coupled to the field equations for a Gaussian incident beam, as shown in sections 2–5 of this review.

As has been pointed out by Firth (1990) and Grynberg (1988), optical systems with a diffusive nonlinearity involve a reaction–diffusion equation. Reaction–diffusion processes occur whenever species react under conditions of non-uniform concentration and are involved in phenomena as diverse as flame front propagation, chemotaxis and biological differentiation. In general, they are governed by systems of equations which include nonlinear or coupled diffusion equations for the concentrations of one or more species, which specify the state of the system. In thermo-optic systems (i.e. those in which the refractive index depends on temperature), the primary state variable is temperature; spatio-temporal variations in temperature are transformed into spatio-temporal patterns in reflected and transmitted light, which may be observed in both near and far field. Spatio-temporal patterns in the state variable may thus be monitored visually as in the well known Belousov–Zhabotinsky system.

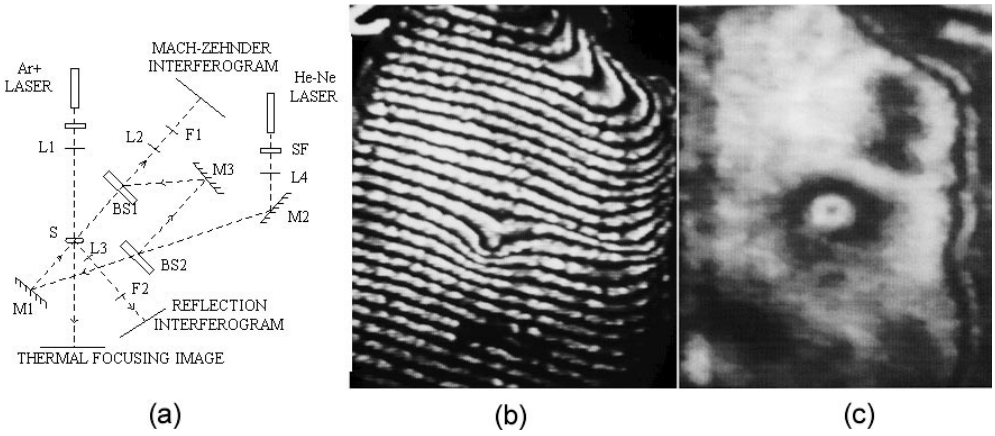

Figure 4. (a) Experimental setup for interferometric measurement of the temperature in a PMN Fabry–Pérot resonator undergoing thermal focusing oscillations (O'Sullivan *et al* 1996b). (b) Multiple reflection interferogram produced by a 0.74 mm PMN crystal, 60 seconds after switching on a steady 0.295 mW argon beam of beamwidth 28 μm at the sample (O'Sullivan *et al* 1996b). (c) Mach–Zehnder interferogram under the same conditions.

Conditions for the occurrence of patterns, waves and oscillations in reaction–diffusion systems are discussed in the monographs by Grindrod (1991) and Kerner and Osipov (1994).

The oscillatory phenomena in the ferroelectrics PMN and PLZT have been explained qualitatively in terms of optical bistability (OB) arising from intrinsic Fabry–Pérot resonance (Chen *et al* 1994, Krumins *et al* 1994, O'Sullivan *et al* 1995, Zheng *et al* 1995). One-dimensional plane wave nonlinear etalon models had earlier been used to describe optical bistability in interference filters, bulk semiconductors and multiple quantum-well systems (Smith *et al* 1984, Dagenais *et al* 1985, Miller *et al* 1981, Yokoyama 1989). Using a finite element solution of the slowly varying envelope equations for the light fields in a Fabry–Pérot etalon under Gaussian illumination, Chen *et al* (1994) derived theoretical curves for steady state bistability and time dependent transmitted power which qualitatively matched experimental results. Since their model used an incorrect temperature profile, however, it did not provide a quantitative fit and was unable to match qualitatively the time dependence of the central irradiance in figure 2. Furthermore, no systematic explanation has been provided for the quantitative dependence of the switching times and spatial structure of the transmitted beams on sample properties, input power and beam diameter and the existence of a threshold (which is absent in thermal focusing).

In PMN and PLZT the threshold for oscillations is quite different from the threshold for the appearance of the first minimum in the thermal lens pattern, for example in PMN:

(1) To within a factor of two, the thermal lens pattern has the same power threshold for an unfocused beam (diameter 2 mm) as for beam focused by a 15 cm focal length lens (diameter $\sim$40 μm). On the other hand, the power threshold for oscillations for the focused beam is $\sim$100 mW whereas there are no oscillations for powers $<$1 watt for the unfocused beam. Above the oscillation threshold, as shown in figure 5, a plot of transmitted power versus incident power (Chen and Scott 1993b) exhibits optical bistability with several hysteresis loops.
(2) With a focused beam, oscillations disappear when the angle of incidence is increased to the point where overlap of internally reflected beams falls below $\sim$50%, whereas the thermal lens pattern is almost unchanged.

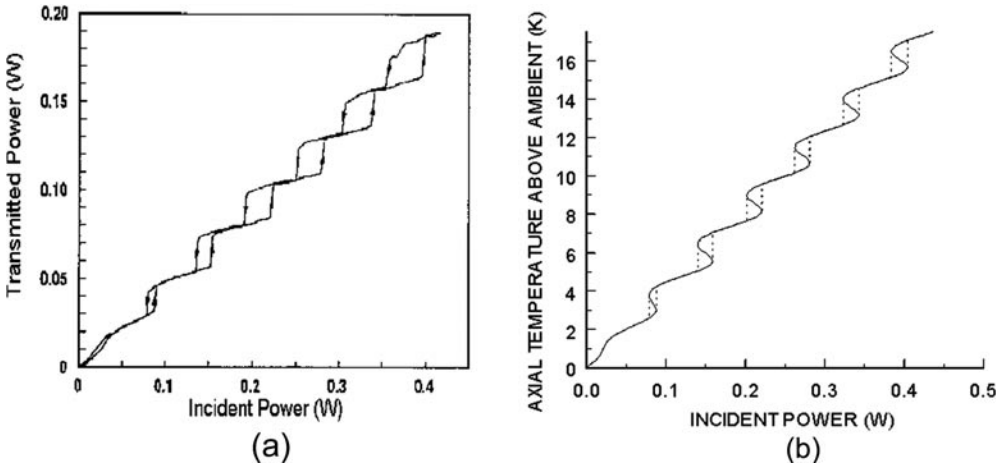

Figure 5. (a) Bistability curve of transmitted power versus incident power for 0.43 mm ceramic PMN (Chen and Scott 1993b). (b) Bistability curve for the steady state axial temperature versus incident power from equation (4.2) for the same experimental parameters as in (a).

Although the phenomena described here are intrinsically slow (ms) due to the thermal time constants involved, and consequently are of little interest for ns or ps photonic switching systems, they nevertheless provide several real commercial applications: First among these is the their use as intra-cavity noise reduction devices for argon ion lasers. At present the preferred scheme for noise limitation in such lasers is to use an extra-cavity feedback system consisting of fast electronics. However, it has already been demonstrated (Ozolinsh *et al* 1997) that a thick film of PMN or PLZT inserted into the etalon holder for a single-mode argon laser (figure 6(a)) provides a cheap, robust and reliable feedback element with $>80\%$ noise reduction (figure 6(b)). This passive device simply causes beam divergence when the power level fluctuates upwards and beam convergence when it fluctuates downwards. Both single crystals and pressed ceramic discs can be used for this application, in which a cheap passive device replaces an active system of fast feedback electronics. Second is the use of the switching times of thermal relaxation oscillations to obtain direct information on the temperature dependence of thermal conductivity and thermo-optic coefficient of ferroelectrics near their phase transition. Third is the use for pedagogical purposes: classroom lecture demonstrations of optical bistability and regenerative pulsations often involve simulations (such as Duffing oscillators). PMN thick films, when combined with the Ar^+ lasers readily available in most universities for classroom or laboratory demonstrations, give an easy and very reliable real demonstration in which the oscillation period can be varied over wide range. Moreover the effect is visually spectacular, both because the frequencies of 1–50 Hz are ideal for the human eye and the colour and intensity are optimum for viewing. Fourthly, the frequencies for regenerative pulsation in these devices are very sensitive to air pressure and flow rate, due to the convective heat transfer at the sample surfaces. It is notable that this purely photonic device (no wires in or out) can sense 0.1 Torr absolute pressure. Therefore prototype optical flow gauges were made capable of measuring, by laser beams only, flow rates as low as 0.003 $m^3\ h^{-1}$ at 1 atm (Scott and Chen 1992)—see figure 7. Fifthly, it was recognized as early as 1984 that optical bistability could be used as a temperature sensor (Miller 1984, Jaeger *et al* 1985, Lambsdorff *et al* 1986) with reduction to practice demonstrated with Ar laser-pumped CdS (Grohs *et al* 1990, Wegener and Klingshirn 1987, Haddad *et al* 1986). Recently these

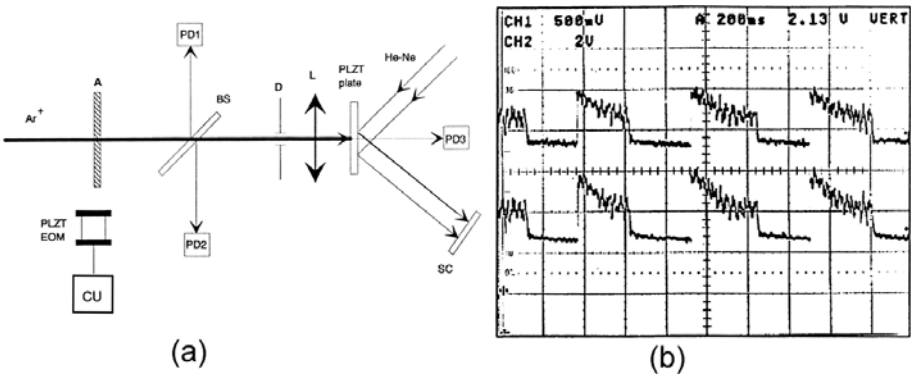

Figure 6. (a) Block diagram of thermal focusing ferroelectric plate inserted as a passive noise-limiter in an argon-ion laser (Ozolinsh *et al* 1997). (b) Noise reduction (∼80%) in an argon-ion laser feedback circuit using ferroelectric thermal focusing, as shown in (a) (Ozolinsh *et al* 1997).

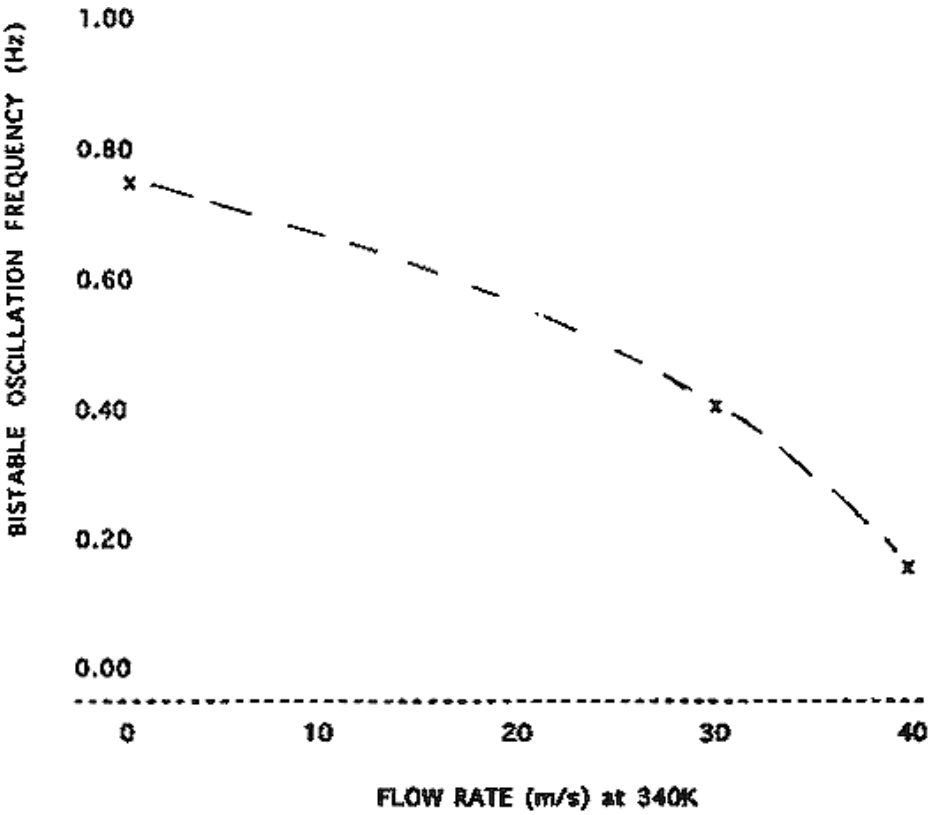

Figure 7. Average oscillation frequency for a ceramic PMN sensor against flow rate of ambient air (Scott and Chen 1992).

phenomena in PMN and PLZT have been under study in Sweden (Ozolinsh *et al* 1997), Japan (Chen *et al* 1995) and Latvia (Krumins *et al* 1994, 1995, 1996) as well as in the USA and Australia (O'Sullivan *et al* 1995, Zheng *et al* 1995).

Thermal lensing in photorefractive media, such as high-dielectric oxides, is of particular interest because, as Bannerjee *et al* (1995) have pointed out, thermal focusing or defocusing provides a transverse instability that can initiate holographic self-assembly of patterns via optical generation of micron-sized charged defect waves. The relationship between optical bistability and pattern self-assembly in ferroelectrics (Grynberg 1988, Firth 1990, Honda 1995, Scott and O'Sullivan 1996, Scott *et al* 1996) is currently under investigation.

In this paper we show that the spatio-temporal characteristics of the transmitted and reflected beam patterns observed experimentally when a parallel-sided slab of absorbing thermo-optic material is heated by a Gaussian laser beam can be explained quantitatively by a thermally diffusive nonlinear etalon model. For sufficiently high values of the coefficient of finesse and moderate values of $\mathrm{d}n/\mathrm{d}T$, the beam exhibits relaxation oscillations, as observed in PMN (figure 2) and PLZT for sufficiently high incident power. For large $\mathrm{d}n/\mathrm{d}T$ or negligible finesse, on the other hand, the model predicts the smooth oscillations observed in BNN and Ce:SBN (figure 3). In section 2 we describe the model and an iterative scheme for solving the heat equation coupled to the slowly varying wave equations. In section 3.1 we show that the temperature profile for typical experimental parameters is almost independent of the axial coordinate z. Hence the radial temperature profile averaged over sample thickness may be used to derive the r and z dependent beam profiles. In section 3.2 we derive the spatio-temporal temperature profile for typical experimental conditions. In section 4 we use the analytical solution for the radial temperature profile to derive quantitatively the switching times bistability curves and compare with experiment. In section 5 we solve the slowly varying envelope equations for a Gaussian incident beam to obtain computed profiles for the transmitted and reflected beams, which are compared with experiment. The results are discussed in section 6.

2. Diffusive nonlinear etalon model

The propagation of light through thick nonlinear media has been studied by numerical techniques under a range of conditions (Wagner *et al* 1968, Gibbs *et al* 1981, Abraham and Firth 1990). Both the equations for the light field and the equation for the nonlinear parameter contain time derivatives and analytic solution is not possible in general. Nor has a general analysis been presented of the qualitative behaviour observed in different parameter regimes. It has been shown by Weaire *et al* (1985) that OB disappears above a critical Fresnel number $\mathcal{F}_c$, i.e. above a critical sample thickness for given incident beamwidth (see also Weaire and Kermode 1986). This was observed experimentally by O'Sullivan *et al* (1995) in PMN and is due to the fact that above $\mathcal{F}_c$ the beam divergence within the sample due to diffraction is so large that Fabry–Pérot resonance does not occur uniformly across the beam. Hence, in this paper we consider dispersively nonlinear materials, whose thickness is less than the waist length of the incident beam but not necessarily so thin that the thin lens approximation (Bjorkholm *et al* 1982, Khoo *et al* 1984) is valid. The temperature distribution is therefore well approximated by that in a circular disc heated by an axial Gaussian light source of constant beamwidth through the sample, although both the radial and azimuthal variation of the light field in response to the temperature dependent refractive index are retained in the slowly varying wave field equations which determine the thermal lens patterns (Wright *et al* 1985, Firth *et al* 1985). In air or vacuum, the disc is cooled by convection and/or radiation from its faces. For experimentally relevant temperature ranges, the convective and radiative cooling coefficients are combined into a single linearized coefficient in the 'radiation boundary condition' of heat transfer theory (Carslaw and Jaeger 1959).

The equations governing the system are the heat equation (2.1) coupled to Maxwell's equations for the forward and backward travelling light beams in the slowly varying envelope

approximation (SVEA) (2.2) and (2.3) (Firth *et al* 1985, Wright *et al* 1985):

$$K(\nabla_T^2 T + \partial^2 T/\partial z^2) - c\rho \partial T/\partial t = -\alpha_a I_c \tag{2.1}$$

$$\partial E_F/\partial z = -\tfrac{1}{2}\alpha E_F + \mathrm{i}kn(T)E_F + \mathrm{i}(2kn_0)^{-1}\nabla_T^2 E_F \tag{2.2}$$

$$\partial E_B/\partial z = \tfrac{1}{2}\alpha E_B + \mathrm{i}kn(T)E_B - \mathrm{i}(2kn_0)^{-1}\nabla_T^2 E_B \tag{2.3}$$

where z is the axial coordinate and t is time, $\nabla_T^2 = \partial^2/\partial x^2 + \partial^2/\partial y^2$ is the transverse Laplacian, which equals $\{\partial/\partial r(r\partial/\partial r)\}/r$ in the radially symmetric case, $T(r, z, t)$ = temperature increment above ambient within the resonator, with the initial condition $T(r, z, 0) = 0$, L = disc thickness, c = specific heat, ρ = density, K = thermal conductivity and $I_c(r, z, t)$ is the beam intensity within the sample; $E_F(r, z) = E_{0F}(r, z)\exp\{\mathrm{i}kn_0 z - \alpha z/2\}$ and $E_B(r, z) = E_{0B}(r, z)\exp\{-\mathrm{i}kn_0 z + \alpha z/2\}$ are the time-independent parts of the light fields of the forward and backward travelling waves within the Fabry–Pérot resonator respectively; α = extinction coefficient $= \alpha_a + \alpha_s$, where α_a = absorption coefficient, α_s = scattering coefficient, k = free space wavenumber $= 2\pi/\lambda$, λ = free space wavelength, n_0 = refractive index at $T = 0$. Hence $I_c(r, z, t) = (n/\mu_0 c_0)|E_F + E_B|^2$, where μ_0 and c_0 are the vacuum permeability and light speed respectively. Since the light transit time through the sample is many orders of magnitude shorter than the thermal time scales, we may assume that the electric field distribution within the sample adjusts instantaneously to changes in the refractive index $n(T)$ according to equations (2.2) and (2.3). For a thermo-optic material with a dispersive nonlinearity due to a temperature-dependent refractive index, the optical thickness is

$$nL = n_0 L_0[1 + \{(\mathrm{d}n/\mathrm{d}T)/n_0 + (\mathrm{d}L/\mathrm{d}T)/L_0\}T] \equiv n_0 L_0(1 + \chi T) \tag{2.4}$$

where $(\mathrm{d}n/\mathrm{d}T)/n_0$ is the thermo-optic coefficient and $(\mathrm{d}L/\mathrm{d}T)/L_0$ the linear expansion coefficient. For thermo-optic materials such as PMN and PLZT, $(\mathrm{d}n/\mathrm{d}T)/n_0$ is an order of magnitude larger (Korshunov *et al* 1992, Chen *et al* 1994) than $(\mathrm{d}L/\mathrm{d}T)/L_0$ so we may write: $\chi \cong (\mathrm{d}n/\mathrm{d}T)/n_0$. In this model, we assume that χ and the thermal conductivity K are constant over the temperature range of the experiment. The thermo-optic coefficient is effectively constant over a range of about 20 degrees in the vicinity of the ferroelectric phase transition in relaxor ferroelectrics, such as PMN and PLZT (Korshunov *et al* 1992), but exhibits a cusplike dependence on temperature in displacive transitions. Effects due to possible temperature dependence of $\mathrm{d}n/\mathrm{d}T$ and K will be considered in sections 4.2 and 6.

The boundary conditions for the system of equations (2.1)–(2.3) for the region $0 \leqslant z \leqslant L$ are:

$$K\partial T(r, z, t)/\partial z|_{z=0,L} = \pm H T(r, z, t)|_{z=0,L} \qquad \text{(the 'radiation boundary condition')} \tag{2.5}$$

$$\partial T(r, z, t)/\partial r|_\Omega = 0 = T(r, z, t)|_\Omega \tag{2.6}$$

$$\sqrt{R}E_B(r, 0) = E_F(r, 0) - \mathcal{T}E_i(r) \qquad E_B(r, L) = \sqrt{R}E_F(r, L) \tag{2.7}$$

$$E_B(r, 0)|_\Omega = E_F(r, 0)|_\Omega = 0 \tag{2.8}$$

where Ω represents a sufficiently distant boundary in the transverse plane (e.g. $r = a$ where $a \gg w$, but it is not necessary to assume radial symmetry at this stage), $E_i(r) = (2\mu_0 c_0 P/\pi w^2)^{1/2}\exp(-r^2/w^2)$ = incident amplitude, P = incident laser power, R = reflectance, $\mathcal{T}$ = amplitude transmission coefficient and $H = H_c + H_r$ is the linearized heat transfer coefficient from the disc surfaces, which may be taken as constant for moderate temperature differences, H_c and H_r being the linearized coefficients for convection and radiation respectively. We assume the front face of the sample to be at the incident beam waist. Without loss of generality we take the initial Fabry–Pérot detuning to be zero.

The system of nonlinear coupled partial differential equations (2.1)–(2.3) with the boundary conditions (2.5)–(2.8) cannot be solved exactly in closed form, nor have numerical

solutions been obtained for the full system, but only for simpler related systems, using either finite difference methods or fast Hankel transforms (Gibbs 1985, Wright *et al* 1985, Firth *et al* 1985). Furthermore questions of the nature of solutions in different parameter regimes, including the existence of periodic solutions, have not been addressed. Periodic oscillations are well known both in active optical resonators, such as lasers, and in passive optical systems including gases and semiconductors (Gibbs 1985). To discover whether periodic solutions of equations (2.1)–(2.3) exist in some region of parameter space, however, neither numerical solution nor experiment are immediately useful, since there are at least eight variable parameters: α, L, k, n_0, $\mathrm{d}n/\mathrm{d}T$, w, $c\rho$ and K. This issue is discussed further in relation to equations (2.9) to (2.11).

Furthermore, symmetry breaking from radially symmetric to hexatic structures has been observed experimentally in the beam transmitted from a PMN crystal (Scott and O'Sullivan 1996) and similar phenomena have been observed in other systems involving different absorption and diffraction mechanisms (Grynberg 1988, Firth 1990, MacDonald and Eichler 1992, Honda 1993). An understanding of these phenomena requires analysis of the stability of the radially symmetric solutions of equations (2.1)–(2.3) under non-radially symmetric spatial perturbations. In this paper we analyse the radially symmetric model; radial symmetry breaking will be treated in a separate paper. Note that the onset of spatial chaos in thermal focusing and the threshold for formation of a turbulent boundary layer was first developed by Firth (1987); this is unrelated to the effective 'optical Reynolds number' (defining the similarity of the thermal lensing of short pulses) derived by Steverding (1976).

Assuming radial symmetry, we introduce the dimensionless independent variables $u = r/w$, $\zeta = z/L$ and $\tau = t/t_K = Kt/c\rho w^2$, so that equations (2.1)–(2.3) become

$$\nabla_u^2 T + (w/L)^2 \partial^2 T/\partial \zeta^2 - \partial T/\partial \tau = -\alpha_a w^2 I_c/K \tag{2.9}$$

$$\partial E_F/\partial \zeta = -\tfrac{1}{2}\alpha L E_F + \mathrm{i}kLn(T)E_F + \mathrm{i}(\mathcal{F}/2)\nabla_u^2 E_F \tag{2.10}$$

$$\partial E_B/\partial \zeta = \tfrac{1}{2}\alpha L E_B - \mathrm{i}kLn(T)E_B - \mathrm{i}(\mathcal{F}/2)\nabla_u^2 E_B \tag{2.11}$$

where $\nabla_u^2 = \{\partial/\partial u(u\partial/\partial u)\}/u$ and $\mathcal{F} = L/kn_0 w_0^2$ is the Fresnel number, which gives a measure of the change in beam diameter within the sample due to diffraction. $\mathcal{F}$ is typically less than 0.03 for samples of thickness $\leqslant 1$ mm, whereas $kLn_0 \sim 2 \times 10^5$ and $kL(\mathrm{d}n/\mathrm{d}T)$, which is responsible for the change in beam diameter due to thermal focusing, is about 20. Hence the Laplacian term in equations (2.10) and (2.11) constitutes a small perturbation and makes an insignificant contribution to the temperature profile.

Characterization of the possible solutions of the system described by equations (2.9)–(2.11) for various parameter ranges requires a stability analysis of the steady state solutions. Equation (2.9) indicates that heat flow from the centre of the disc is predominantly radial or axial for $w^2/L^2 \ll 1$ or $\gg 1$ respectively. Most experiments to date have been carried out under the condition $w^2/L^2 \ll 1$, which suggests that the ζ-dependence of the temperature may be negligible. In fact, we show in appendix A that the spatio-temporal solution of equation (2.1) with I_c replaced by a steady Gaussian heat source switched on at time $\tau = 0$ in a typical sample disc is independent of ζ to within 1%. We show in section 3.2 that, without ζ-dependence of temperature, the system exhibits bistability without periodic solutions. In a separate paper (O'Sullivan, to be submitted), we show that the ζ-dependent temperature profile given by equations (2.9)–(2.11) is characterized by a bifurcation parameter. Below the first bifurcation point the system possesses a single asymptotically stable steady state temperature. At the first bifurcation point the steady state solution becomes bistable and at the second bifurcation point, Hopf bifurcation to a periodic solution can occur near the turning points of the bistability curve.

Experimental observations of bistability and aperiodic oscillations in ferroelectrics to date have been carried out for parameter values between the first and second bifurcation points. In this parameter range the ζ-dependence of the temperature has no qualitative effect and no significant quantitative effect on the observed system behaviour. Hence the system can be modelled accurately by integrating equation (2.1) or (2.9) over sample thickness to obtain a heat balance equation for the temperature average over sample thickness $\bar{T}(u, \tau)$ and using it for the temperature in the term $n(T)$ in equations (2.2), (2.3), (2.10) and (2.11). Furthermore, although the transverse Laplacian terms in equations (2.10) and (2.11) are essential for determining the diffraction of the laser beam and hence the transmitted beam patterns, the low Fresnel number implies that diffraction is small and, in any case, is opposed by thermal focusing. Hence it makes a negligible difference to the *heating effect* of the beam. Hence for the parameter range of the above experiments, we solve equations (2.9) to (2.11) by means of the following self-consistent approximation procedure.

(i) In the zeroth iteration (section 3.2) the u, τ-dependent heat source term $\alpha_a I_c$ is obtained by solving equations (2.10) and (2.11) neglecting the ∇_u^2 terms and treating u, τ as parameters, to obtain the familiar Airy function for the temperature dependence of I_c within an envelope given by the Gaussian radial dependence of the incident beam.

(ii) The heat balance equation obtained by integrating equation (2.9) with respect to ζ is then solved using the zeroth order source function $\alpha_a I_c(u, \tau)$ from step (i) to obtain the time dependent axially averaged radial temperature profile $\bar{T}(u, \tau)$.

(iii) In section 5 the temperature profile from step (ii) is then substituted into equations (2.10) and (2.11), which are then solved in the first iteration (including the ∇_u^2 terms) to determine the phase and amplitude of $E_F(r, z)$ and $E_B(r, z)$ and to verify the initial assumption of step (i). This first iterative solution for the propagating beams is then used to determine the transmitted beam patterns in the near and far field.

The analytic temperature profiles obtained by this procedure not only allow quantitative prediction of the transmitted and reflected beam patterns, but also elucidate the functional relationships between the various parameters involved.

3. Temperature profiles

3.1. $T(u, \zeta, \tau)$ for Gaussian heating with constant absorption factor

In appendix A we derive the Green function for equation (2.9) with I_c steady for a disc of infinite radius subject to the 'radiation boundary condition' at its faces. This Green function is then used to obtain the solution $T(u, \zeta, \tau)$ for Gaussian beam heating with constant absorption factor and hence the steady state axial solution $T(u, \zeta)$. Figures 8(a) and 8(b) show plots of $T(u, 0, \tau)$ and $T(0, \zeta, \infty)$, based on equations (A.10) and (A.12). The maximum axial variation of $T(0, \zeta, \infty)$ and hence of $T(u, \zeta, \tau)$ for typical sample thicknesses is less than 1% of the difference between the central temperature and the surroundings as, for example, in figure 8(b).

For typical experimental parameters (see section 3.2), $h \ll 1$ and hence equation (A.4) implies that $\beta_1^2 \to 2h$ and $\beta_m \to 2\pi(m-1)$ for $m \geqslant 2$, so equation (A.10) reduces to

$$T(u, \varsigma, \tau) = \frac{2P_{abs}\cos(\bar{\varsigma}\sqrt{2h})}{\pi LK} \int_0^\tau \frac{\mathrm{d}\tau'}{1+8\tau'} \exp\left(-\frac{2u^2}{1+8\tau'} - \mu^2\tau'\right) \qquad (3.1)$$

where $\bar{\varsigma} = \varsigma - 1/2$ and $\mu^2 = 2w^2H/LK$. $T(u, \zeta, \tau)$ is symmetric in $\bar{\varsigma}$ for typical values of $\alpha_a L$ (e.g. $\alpha_a L = 0.03$ in a typical PMN sample); for larger values of $\alpha_a L$, combination

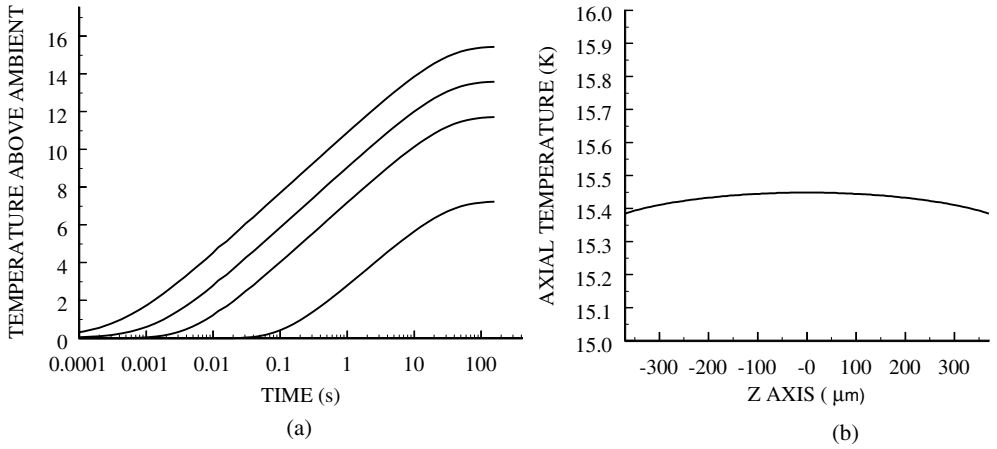

Figure 8. (a) Smoothed temperature evolution for a 0.74 mm thick PMN crystal under steady 295 mW irradiation with a beamwidth 28 μm at 514.5 nm, as calculated from equation (A.10). (b) z dependence of axial temperature at steady state for the sample and conditions of (a), according to equation (A.12).

of $I_c(u, \zeta, \tau)$ with equation (A.3) shifts the maximum of $T(u, \zeta, \tau)$ towards the front face of the sample. For $\bar{\zeta} = 0$, equation (3.1) agrees with the ζ-independent result derived using the Hankel transform in O'Sullivan *et al* (1996b) (note sign correction and redefinition of t_K) for the smoothed temperature profile (i.e. the profile smoothed on a time scale large compared with t_K). Equation (3.1) contains two time scales: the conduction time scale t_K, which determines the establishment of the radial profile for $u \leqslant 1$, and the convection–radiation time scale $t_c = t_K/\mu^2 = \rho c L/2H$, which determines the relaxation time of the whole system to steady state. Similarly, equation (A.10) contains multiple time scales: t_K and $t_{cm} = L^2/\kappa\beta_m^2$ ($m = 1, 2, 3, \ldots$). For typical experimental parameters, the small argument approximation applies for $m = 1$ in the equation for β_m so that t_{c1} equals t_c and is about four orders of magnitude greater than t_K. Setting u, $\bar{\zeta} = 0$ in equation (3.1) gives the central sample temperature as a function of time in closed form:

$$T(0, 0, \tau) = (P_{abs}/4\pi LK)\exp(t_K/8t_c)[E_1(t_K/8t_c) - E_1\{(1 + 8\tau)t_K/8t_c)\}] \tag{3.2}$$

where E_1 is the exponential integral function. Unlike earlier work (Gordon *et al* 1965, Whinnery *et al* 1967), which ignored convection–radiation cooling, this result gives a finite steady state temperature. For $t \ll t_c$, equation (3.1) tends to Gordon's non-convective result uniformly on $0 \leqslant u < \infty$, since the time dependence of both expressions reduces to $\ln(1 + 8\tau)$. Furthermore since the earlier analysis yielded a single characteristic time, it could not describe even qualitatively the switching phenomena observed. We note parenthetically that a relaxation equation was also used to describe the temperature within the illuminated region of semiconductor systems exhibiting absorptive bistability by several authors (Hajto and Janossy 1983, Gutowski *et al* 1989, Wegener and Klingshirn 1987, Haddad *et al* 1986, Kretzschmar *et al* 1987).

The Green function derived in appendix A can be used to derive integral equations for the cases in which I_c is not constant, but in section 3.2 we use an alternative Hankel transform approach.

3.2. $T(u, \tau)$ for Gaussian heating with time-varying absorption in thin samples

As shown in figure 8(b), the gradient of $T(u, \zeta, \tau)$ in the ζ direction is small. Its maximum value occurs at the surfaces $\zeta = 0, 1$, where the conductive heat flux matches the heat flux to the surroundings given by Newton's law of cooling: $K\partial T(u, \zeta, \tau)/\partial\zeta|_{\zeta=0,1} = \pm HL\bar{T}(u, \tau)$ where H may be taken as constant for moderate temperature differences and $\bar{T}(u, \tau)$ is the temperature averaged over the thickness of the disc. We therefore integrate each term in equation (2.9) with respect to ζ to obtain the heat balance equation:

$$\partial^2 T/\partial u^2 + (\partial T/\partial u)/u - \partial T/\partial\tau = (-I_{abs} + 2HT)w^2/LK \tag{3.3}$$

where $T(u, \tau)$ now represents $\bar{T}(u, \tau)$ and $I_{abs}(u) = \int_0^1 \alpha_a I_c(u, \varsigma)\,\mathrm{d}\varsigma$ = absorbed beam intensity. For a disc radius much greater than the beamwidth of the incident beam, the boundary conditions on $T(u, \tau)$ may be taken as $\partial T(0, \tau)/\partial u = 0$ and $T(\infty, \tau) = 0$. Physically equation (3.3) means that the rate of temperature increase within an annular slice of radius u is proportional to net heat inflow into the slice.

Neglecting the transverse Laplacian terms and treating u, τ as parameters in the term $n\{T(u, \tau)\}$, equations (2.10) and (2.11) can be solved with the boundary conditions (2.7) and (2.8) for an incident Gaussian beam to give the intracavity irradiance averaged over several wavelengths:

$$I_c(u, \varsigma) = \frac{I_i(u)(1 - R)F_\alpha\,\mathrm{e}^{\alpha L}\{\mathrm{e}^{-\alpha L\varsigma} + R\,\mathrm{e}^{\alpha L(\varsigma-2)}\}}{4R[1 + F_\alpha \sin^2\{kn(T)L\}]} \equiv A(u, \varsigma, \tau)I_i(u) \tag{3.4}$$

where $F_\alpha = 4R\,\mathrm{e}^{-\alpha L}/(1 - R\,\mathrm{e}^{-\alpha L})^2$ is the coefficient of finesse, $I_i(u) = I_p \exp(-2u^2)$ is the incident beam irradiance and $A(u, \varsigma, \tau)$ is the absorption factor. Setting $u = 0$ in equation (3.4) corresponds to the plane wave case for which optical bistability has been extensively studied (Gibbs 1985, Felber and Marburger 1976, Marburger and Felber 1978). From equation (3.4) we obtain

$$I_{abs}(u, \tau) = \frac{\alpha_a I_i(u)(1 - R)F_\alpha(\mathrm{e}^{\alpha L} - 1)(1 + R\,\mathrm{e}^{-\alpha L})}{4\alpha R[1 + F_\alpha \sin^2\{kL(n_0 + T(u, \tau)\,\mathrm{d}n/\mathrm{d}T\}]} \equiv A(u, \tau)I_i(u). \tag{3.5}$$

In general $A(u, \tau)$ depends on u and τ only through the dependence of α and n on $T(u, \tau)$. This includes the case of negligible finesse (e.g. for Ce:SBN), in which equation (3.5) reduces to the single-pass absorbed intensity, $I_{abs}(u, \tau) = I_i(u)(1 - \mathrm{e}^{-\alpha(u,\tau)L})(1 - R)\alpha_a/\alpha$ and the cases of BNN, PMN and PLZT where α and α_a may be taken as constant over the relevant temperature range. In the case of systems with negligible finesse, such as Ce:SBN, the actual temperature profile is given by equations (3.1) and (3.2), but for PMN and PLZT solution of the nonlinear system of equations (3.3) and (3.5) is required. BNN is discussed below.

O'Sullivan *et al* (1996b) presented smoothed solutions of equations (3.3) and (3.5) obtained by replacing $A(u, \tau)$ by the constant absorption factor A_s, equal to the average of $A(u, \tau)$ on a time scale large compared to t_K. In this paper we present solutions which include the effect of the spatio-temporal dependence of $A(u, \tau)$. We have solved equations (3.3) and (3.5), with the initial condition $T(u, 0) = 0$, by two methods:

(i) numerically by the finite element method for a disc of finite radius and
(ii) analytically for a disc of infinite radius.

Figure 9(a) shows the finite element solution for $T(u, \tau)$ obtained for experimental parameter values for monocrystalline PMN: $\rho = 8120$ kg m^{-3} (Landolt–Börnstein 1961), $c = 335$ J kg^{-1} K^{-1} (Scott and Chen 1992), $R = 0.20$, $\alpha = 120$ m^{-1} (hence $F_\alpha = 1.1$), $n_0 = 2.65$ for $\lambda = 514.5$ nm, disc radius = 1.5 mm, $(\mathrm{d}n/\mathrm{d}T)/n = 9 \times 10^{-5}$ K^{-1} and $(\mathrm{d}L/\mathrm{d}T)/L = 6 \times 10^{-6}$ K^{-1} over the temperature range 280–320 K (Korshunov *et al* 1992,

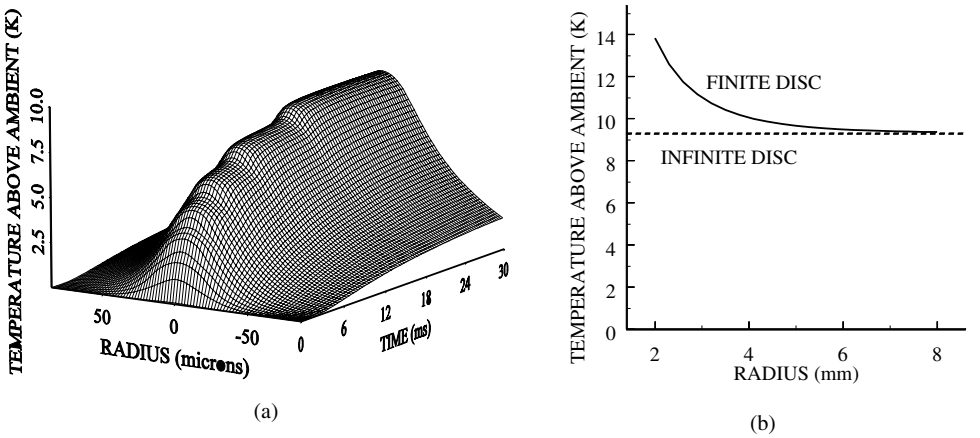

Figure 9. (a) Temperature evolution for a 0.74 mm thick PMN crystal under steady 295 mW irradiation with a beamwidth of 28 μm at 514.5 nm, as given by the finite element model. (b) Steady state axial temperature versus sample radius. The dotted line shows the infinite disc approximation.

Chen *et al* 1994) and $H = 22.5$ W m^{-2} K (O'Sullivan *et al* 1996b). The values of K and α_a have not been directly measured. The values $K = 0.65$ W m^{-1} K^{-1} and $\alpha_a/\alpha \cong 0.3$ used in plotting figure 9(a) and later figures in this paper were determined by fitting analytic steady state solutions to experimental results (O'Sullivan *et al* 1996b) and the value of K so determined agrees well with that of other ABO_3 perovskites. As expected on the basis of the two time scales which occur in equation (3.1), figure 9(a) shows that the temperature equilibrates with an overall timescale t_c through a sequence of metastable states separated by jumps with the much shorter timescale t_K.

Figure 9(b) compares the steady state axial temperature for an infinite radius disc, given by equation (3.1), with that for a finite disc as a function of radius, using the same smoothed absorption factor A_s, based on equation (9) of O'Sullivan *et al* (1996b):

$$T(u) = T(0)I_0(\mu u) + \frac{2A_\infty P}{\pi LK}\left\{K_0(\mu u)\int_0^u \mathrm{d}u'\,u' I_0(\mu u')\,\mathrm{e}^{-2u'^2} - I_0(\mu u)\int_0^u \mathrm{d}u'\,u' K_0(\mu u')\,\mathrm{e}^{-2u'^2}\right\} \tag{3.6}$$

where

$$T(0) = (2A_\infty P/\pi LK)\left\{[K_1(\mu b') - (L\mu/2w)K_0(\mu b')]/[I_1(\mu b') + (L\mu/2w)I_0(\mu b')] \times \int_0^{b'} \mathrm{d}u'\,u' I_0(\mu u')\,\mathrm{e}^{-2u'^2} + \int_0^{b'} \mathrm{d}u'\,u' K_0(\mu u')\,\mathrm{e}^{-2u'^2}\right\}$$

$b = b'w$ = disc radius, A_∞ = steady state absorption factor and K_0, K_1, I_0 and I_1 are modified Bessel functions of the second and first kinds respectively. Although edge effects lead to an underestimation of temperature for small samples, figure 9(b) shows that they are insignificant above a radius of 6–8 mm for a typical experimental beamwidth. Hence, in order to investigate the parameter dependence of the time-dependent solution of equations (3.3) and (3.5), it is useful to investigate their solution for an infinite disc.

Taking the Hankel transform of equation (3.3), we obtain

$$\partial\tilde{T}/\partial\tau = -(s^2 + \mu^2)\tilde{T} + I_p w^2 G(s,\tau)/LK \tag{3.7}$$

where, $\tilde{T}(s,\tau) = \int_0^\infty \mathrm{d}u\, u J_0(su) T(u,\tau)$, J_0 is a Bessel function of order zero and

$$G(s,\tau) = \int_0^\infty \mathrm{d}u\, u J_0(su) \exp(-2u^2) A(u,\tau).$$

$A(u,\tau)$ depends on (u,τ) via its dependence on $T(u,\tau) = \int_0^\infty \mathrm{d}s\, s J_0(su)\tilde{T}(s,\tau)$. Proceeding formally, equation (3.7) with the initial condition $\tilde{T}(s,0) = 0$ is equivalent to an integral equation for $\tilde{T}(s,\tau)$:

$$\tilde{T}(s,\tau) = (I_p w^2/LK)\exp\{-(s^2+\mu^2)\tau\}\int_0^\tau \mathrm{d}\tau'\, G(s,\tau')\exp(s^2+\mu^2)\tau'. \tag{3.8}$$

Taking the inverse Hankel transform, we obtain an integral equation for $T(u,\tau)$:

$$T(u,\tau) = \frac{I_p w^2}{LK}\int_0^\tau \mathrm{d}s\, s J_0(su)\int_0^\tau \mathrm{d}\tau'\, \mathrm{e}^{(s^2+\mu^2)(\tau'-\tau)}\int_0^\infty \mathrm{d}u'\, u' J_0(su')\,\mathrm{e}^{(-2u'^2)A(u',\tau')}. \tag{3.9}$$

Reversing the order of integration, we obtain

$$T(u,\tau) = \frac{I_p w^2}{LK}\int_0^\tau \mathrm{d}\tau'\, \mathrm{e}^{\mu^2(\tau'-\tau)}\int_0^\infty \mathrm{d}u'\, u'\,\mathrm{e}^{(-2u'^2)A(u',t')}\int_0^\infty \mathrm{d}s\, s J_0(su) J_0(su')\,\mathrm{e}^{s^2(\tau'-\tau)}.$$

The s integral has the form of Weber's second exponential integral (Watson 1966) so that $T(u,\tau)$ can be expressed as a double integral:

$$T(u,\tau) = \frac{I_p w^2}{LK}\int_0^\tau \mathrm{d}\tau'\, \mathrm{e}^{\mu^2(\tau'-\tau)}\int_0^\infty \mathrm{d}u'\, u'\frac{\mathrm{e}^{(-2u'^2)A(u',t')}}{2(\tau-\tau')}\exp\left\{-\frac{u^2+u'^2}{4(\tau-\tau')}\right\} I_0\left\{\frac{uu'}{2(\tau-\tau')}\right\}.$$

Changing the variable in the time integral to $\nu = \tau - \tau'$ gives

$$T(u,\tau) = \frac{I_p w^2}{2LK}\int_0^\tau \frac{\mathrm{d}\nu}{\nu}\,\mathrm{e}^{(-\mu^2\nu)}\int_0^\infty \mathrm{d}u'\, u' A(u',\tau-\nu)\exp\left(-2u'^2 - \frac{u^2+u'^2}{4\nu}\right) I_0\left(\frac{uu'}{2\nu}\right). \tag{3.10}$$

Equation (3.10) can also be obtained using the ζ-independent limit of the Green function in equation (A.7).

Equation (3.10) is a double integral equation of Volterra type in τ and of Fredholm type in u and is a special case of the equation quoted by Corduneanu (1991). As Corduneanu points out, it may be treated as a Volterra integral equation of the second kind if we regard $T(u,\tau)$ as a variable whose values are functions defined on $0 < u < \infty$. Hence we may apply the standard theorems on existence and uniqueness of solutions of Volterra integral equations. In particular, for a wide range of functions $A(u,\tau)$ representing absorptive and/or dispersive nonlinearities, the integrand of equation (3.10) satisfies the conditions for the existence of a unique solution. Hence any valid solution found numerically is the unique solution. There is a distinct advantage in solving the integral equation (3.10) instead of the partial differential equation (3.3) since the smoothing property of integration means that less stringent regularity conditions are required of trial solutions of integral equations and numerical solution algorithms are less prone to numerically generated errors.

Figure 10(a) shows a contour plot of $T(u,\tau)$ obtained by numerical solution of equation (3.10) using the method of Tonelli (1928) (see below) for typical parameter values. This solution agrees with that obtained by the finite element method (e.g. see figure 9(a) subject to the correction given in figure 9(b) for sample radii <6 mm. Figure 10(a) shows that switching waves, as described by Rozanov (1981), do not occur in these systems. This is because the low Fresnel number satisfies the condition of Moloney and Gibbs (1982) for 'whole beam switching'.

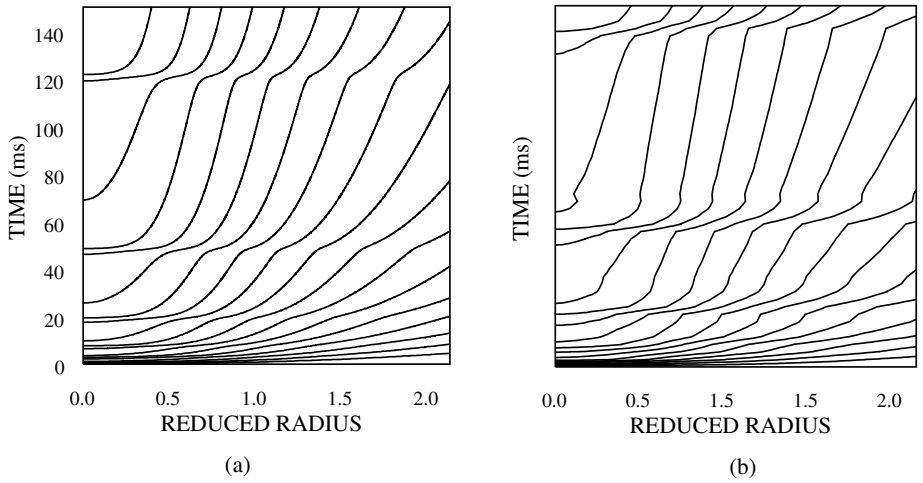

Figure 10. (a) Temperature contours as a function of radius (horizontal axis, 0 to 2 beamwidths) and time (vertical axis, 0 to 30 ms), given by equation (3.10). (b) Temperature contours given by equation (3.12) using the loci defined by equation (3.11).

The essential features of the solution for moderate incident laser power can, however, be computed more rapidly by reducing the right-hand side of equation (3.10) to a single integral as follows. Firstly we note that equation (3.10) contains the temporal convolution of the oscillating function $A(u', \tau - \nu)$ with a kernel which has a single maximum for each point in the ν–u' plane. Since $I_0(x) \sim e^x(2\pi x)^{-1/2}$ as $x \to \infty$, it is useful to reformulate the kernel as

$$\frac{u'}{\nu} \exp\left\{-\mu^2\tau' - \frac{2u^2}{8\nu+1} - 2\left(1+\frac{1}{8\nu}\right)\left(u' - \frac{u}{8\nu+1}\right)^2\right\} \exp\left(-\frac{uu'}{2\nu}\right) I_0\left(\frac{uu'}{2\nu}\right).$$

For fixed u and ν, the function $e^{-x}I_0(x)$ with $x = uu'/2\nu$ decreases from a maximum value of 1 as u' increases from 0 and asymptotes to $1/\sqrt{2\pi x}$ as $x \to \infty$ (Abramowitz and Stegun 1964). Hence as ν increases from zero for each fixed u, the kernel evolves monotonically from a delta function located at $u' = u$ to an approximately Gaussian window of unit width and decreasing height with its peak at $u' = 0.5$.

The value of the integral differs qualitatively in three distinct regimes determined by the temperature difference across the beamwidth, $\Delta T_w = T(0, \tau) - T(1, \tau)$, given by equations (3.1) and (3.6), which is approximately the same for the smoothed and the stepped temperature profiles for $\tau > 1$

(i) For $\Delta T_w < \pi/2kL(dn/dT)$, $A(u', \tau - \tau')$ varies by less than half a cycle across the width of the convolution window for all u and τ', hence the u' integral in equation (3.10) is dominated by the value of $A(u', \tau - \tau')$ at the peak of the window. The locus $u' = u_p(\tau')$ of this peak in the τ'–u' plane for fixed u is given by the solution of the transcendental equation:

$$\{1 - 4(1 + 1/8\tau')u_p^2\}I_0(uu_p/2\tau') + (uu_p/2\tau')I_1(uu_p/2\tau') = 0. \quad (3.11)$$

Representative loci are shown in figure 11(a). Note that $u_p(0) = u$ and $u_p(\infty) = 0.5$ for all u. On replacing $A(u', \tau - \tau')$ by $A\{u_p(\tau'), \tau - \tau'\}$, the u'-integral in equation (3.10)

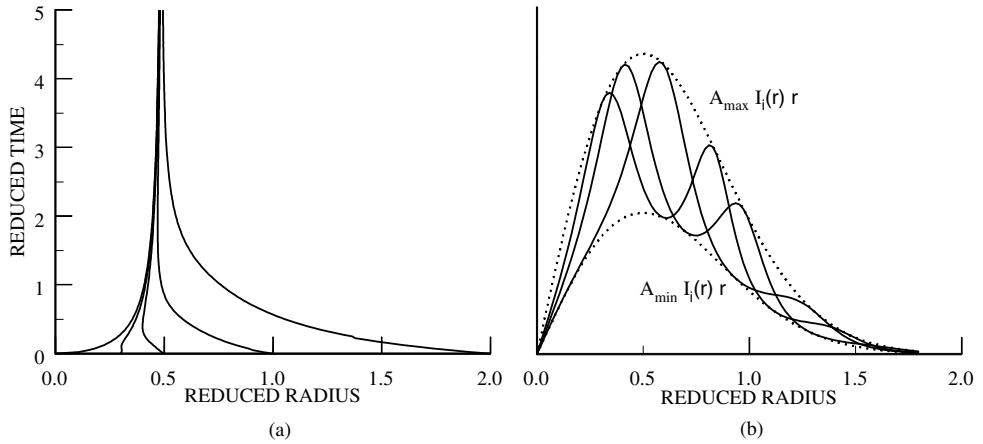

Figure 11. (a) Loci of the peak of the kernel in equation (3.10) in the u', τ' plane. The loci start at $u' = 0$, 0.3, 0.5 and 2. (b) Heat source term $u'A(u', \tau - \tau')\exp(-2u'^2)$ for three representative values of the Fabry–Pérot phase. The dotted lines show the maximum and minimum FP absorption envelopes. Parameters as in figure 8(a).

can be evaluated using equation (A.9) to give

$$T(u,\tau) = \frac{I_p w^2}{LK}\int_0^{\tau}\frac{\mathrm{d}\tau'}{1+8\tau'}A\{u_p(\tau'),\tau-\tau'\}\exp\left(-\frac{2u^2}{1+8\tau'}-\mu^2\tau'\right). \tag{3.12}$$

From a physical viewpoint, as τ' increases the temporal convolution integral in equations (3.10) and (3.12) contains the effects of

(a) the instantaneous absorption rate at (u, τ) (for $\tau' = 0$), plus
(b) the absorption rate for u' between u and 0.5 over recent time (for τ' small) and
(c) the absorption rate at $u' = 0.5$ (at which absorption is maximum for τ' large) over earlier times.

(The kink in loci starting from $u \approx 0.5$ is due to the contribution of the outward radial heat flux.) Note that the contours in figure 10 are approximately parallel to the u' axis for $0 \leqslant u' \leqslant 0.25$. Hence $A\{u_p(\tau'), \tau - \tau'\} \approx A\{0, \tau - \tau'\}$ for $u < 0.5$.

(ii) For $2\pi/kL(\mathrm{d}n/\mathrm{d}T) \geqslant \Delta T_w \geqslant \pi/2kL(\mathrm{d}n/\mathrm{d}T)$, $A(u', \tau - \tau')$ oscillates a few times across the convolution window for $\tau' \geqslant 1$ and $u < 2$. For the experimental parameters given above, there are less than two oscillations as shown in figure 11(b). The u'-integral oscillates approximately in phase with $A\{u_p(\tau'), \tau - \tau'\}$ but the amplitude of oscillation is less than in regime (i). Hence the temporal evolution of the radial integral is similar to that in regime (i) but with A_{max} replaced by $A_{max}\{1-\varepsilon/(1+1/2\tau')\}$ and A_{min} replaced by $A_{min}\{1+\varepsilon/(1+1/2\tau')\}$ for some ε where $0 < \varepsilon < 1$. For an incident power of 295 mW, figure 10(b) shows the temperature contours given by equation (3.12) with $\varepsilon = 0.15$ based on figure 11(b). These contours are similar to those in figure 10(a) given by equation (3.10), with only a slight shift in switching times for small values of τ.

(iii) For $\Delta T_w \gg \pi/kL(\mathrm{d}n/\mathrm{d}T)$, the Laplacian terms in equations (2.10) and (2.11) may no longer be neglected as the length of the beam waist becomes $\leqslant L$ and the wavefronts of the beam become highly curved. Hence the iterative approach outlined in section 2 is no longer valid. As the incident power increases, symmetry breaking occurs and non-circular patterns are generated in the transmitted and reflected beams as described elsewhere (Scott and O'Sullivan 1996, Scott *et al* 1996). For BNN, this is the case even for low incident

power values since dn/dT is very large (approximately 0.1). Since the condition for Fabry–Pérot resonance is not satisfied simultaneously over a significant radius, however, there is no longer a significant temporal variation in the average absorption factor. Hence, the evolution of the central irradiance and total power can be obtained by substituting the smoothed temperature profile of equation (3.1) into equations (2.10) and (2.11) as in the case of negligible finesse.

To investigate the time dependence of the axial temperature, we use the fact that for $u = 0$ and $\Delta T_w < \pi/kL(dn/dT)$, $A(u', \tau - \tau') \approx A(0, \tau - \tau')$ within the convolution window. Making this substitution in equation (3.12), changing the variable to $\tau'' = \tau - \tau'$ and replacing τ'' by τ', we obtain

$$T(0,\tau) = \frac{2P}{\pi LK}\int_0^\tau \frac{d\tau'}{1+8(\tau-\tau')}\exp\{-\mu^2(\tau-\tau')\}A(0,\tau') \equiv \int_0^\tau M\{\tau,\tau',T(0,\tau')\}\,d\tau'. \tag{3.13}$$

For a general temperature dependent absorption factor, this is a nonlinear Volterra integral equation of the second kind. Equation (3.13) has a unique solution, provided the integrand satisfies the Lipschitz condition $|M(\tau,\tau',T) - M(\tau,\tau',T')| \leqslant L(\tau,\tau')|T - T'|$ for $0 \leqslant \tau' \leqslant \tau < \infty$ for some function $L(\tau,\tau')$—see for example theorem 2.1.1 of Hackbusch (1995). In particular this condition is satisfied by $A(0,\tau)$ defined in equation (3.5). The solution is bounded from above by a super-solution and from below by a sub-solution, which may be found analytically by replacing $A(0,\tau)$ in equation (3.13) by A_{max} and A_{min} respectively. In principle the unique solution of equation (3.13) can be found by the iterative technique used in the existence proof which we described previously (O'Sullivan *et al* 1996b). In general, however, the iterative solution is slow to converge. A much more rapidly converging algorithm which yields the solution with arbitrary accuracy is Tonelli's method, in which a sequence of approximate solutions $T_n(0,\tau)$ is constructed by partitioning the τ-axis into n intervals and estimating $T_n(0,\tau)$ on each interval from its values on the preceding intervals (Tonelli 1928).

Numerical evaluation of equations (3.12) and (3.13) by the Tonelli method is shown in figures 12(a) and 12(b). In contrast to the smoothed solution of O'Sullivan *et al* (1996b), this solution shows aperiodic jumps in $T(u,\tau)$ with amplitude decreasing as u increases, in agreement with the finite element solution shown in figure 9(a). Although the effective finesse in equation (3.12) in regime (ii), without the adjustment of A_{max} and A_{min} described above, would be greater than in the exact solution (given by the finite element method and by equation (3.10)), this would only alter the steepness of the aperiodic temperature jumps and not their height. Significantly the temperature jumps are of equal height $\Delta T_j = \pi/kL(dn/dT)$ after about 0.01 s, consistent with the similarity of the jumps in central irradiance and total power of the experimental far field transmitted light pattern shown in figure 2(a) and Chen and Scott (1993b). Figure 12 shows that $T(0,\tau)$ increases slowly while $A\{T(0,\tau)\}$ is near A_{min} and rapidly when it is close to A_{max}. Matching the smoothed temperature profile of equation (3.1) with $P_{abs} = PA_s$ to the stepped profile in figure 12(b) shows that $A_s \approx A_{min}+0.2(A_{max}+A_{min})$.

4. Thermo-optic bistability

4.1. Bistability curves for Gaussian irradiation

Chen and Scott (1993b) have published experimental bistability curves for the steady state power transmitted and reflected by a ceramic PMN sample as a function of incident power—figure 5(a). These differ from traditional bistability curves, such as the bistability curve of temperature against input power obtained in the plane wave thermo-optic case and plots of

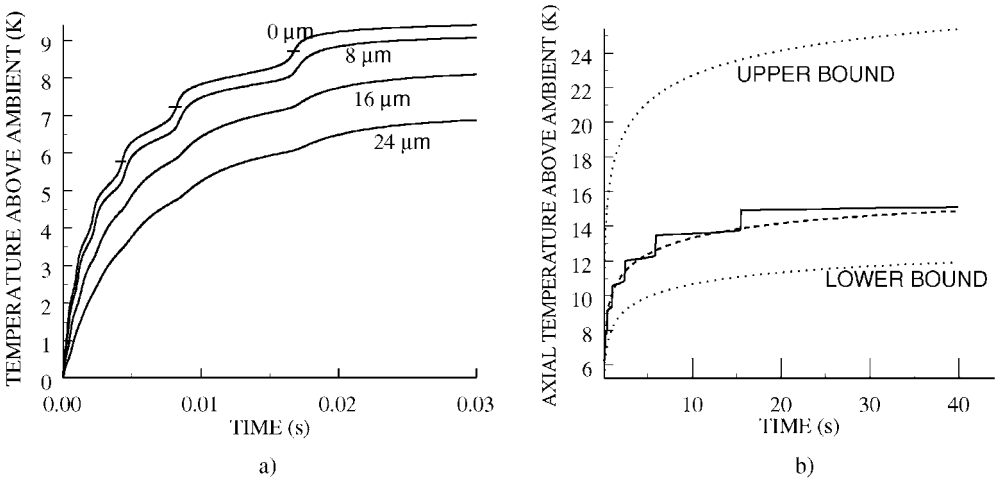

Figure 12. (a) Temperature evolution for a 0.74 mm thick PMN crystal under steady 295 mW irradiation with a beamwidth 28 μm at 514.5 nm, as given by equation (3.12). The dashes indicate the temperature at which maximum absorption occurs. From the top, the curves correspond to $r = 0$, 9, 17 and 26 μm. Other symbols are explained in section 3.2. (b) Central temperature for parameters as (a), over a longer time scale. The dotted lines show the temperature envelope corresponding to maximum and minimum Fabry–Pérot absorption factors A_{max} and A_{min} respectively. The dashed line shows the smoothed solution for $A_s = A_{min} + 0.2(A_{max} - A_{min}) = 52.5 \times 10^{-3}$.

output power against input power for one-dimensional non-diffusive OB, which have a wedge-shaped envelope, so that the width of the hysteresis loops increases monotonically with the control variable. In contrast, the hysteresis loops for Gaussian heating of ferroelectrics have approximately constant width over a wide range of incident power, as shown qualitatively by Chen *et al* (1994).

The steady state bistability curve can be obtained from the inverse Hankel transform of equation (3.7) with $\partial\tilde{T}/\partial\tau = 0$, which gives an integral equation for $T(u, \infty)$:

$$T(u,\infty) = \frac{I_p w^2}{LK}\int_0^\infty \frac{\mathrm{d}s\, s}{s^2+\mu^2} J_0(su)\int_0^\infty \mathrm{d}u'\, u' J_0(su')\exp(-2u'^2)A(u',\infty).$$

The s integral can be evaluated with $u = 0$ to give (Abramowitz and Stegun 1964)

$$T(0,\infty) = (2P/\pi LK)\int_0^\infty \mathrm{d}u\, uK_0(\mu u)\exp(-2u^2)A(u,\infty). \tag{4.1}$$

Assuming that $T(u, \infty)$ has the same u-dependence as the smoothed solution (see section 5),

$$T(u,\infty) = T(0,\infty)\{1 + \mathrm{Ein}(2u^2)/\ln(w^2H/4LK)\} \equiv T(0,\infty)\psi(u) \text{ on } 0 \leqslant u < 2/u$$

equation (4.1) becomes

$$T(0,\infty) = \frac{2PA_{max}}{\pi LK}\int_0^\infty \mathrm{d}u\, \frac{uK_0(\mu u)\exp(-2u^2)}{1 + F_\alpha \sin^2[kL\{n_0 + T(0,\infty)\psi(u)\,\mathrm{d}n/\mathrm{d}T\}]} \equiv P\Psi\{T(0,\infty)\} \tag{4.2}$$

where the function $\Psi\{T(0, \infty)\}$ is independent of P, oscillates with decreasing amplitude as $T(0, \infty)$ increases and can be determined by numerical integration for given values of k, w, H, L, K and $\mathrm{d}n/\mathrm{d}T$. Hence a plot of $T(0, \infty)$ against P gives an S-shaped bistability curve within a lenticular envelope as shown in figure 5(b) for the parameter values given in section 3.2. Since the transmitted amplitude is $E_T(u, 0.5) = \mathcal{T}E_F(u, 0.5)$ where $\mathcal{T}'$ (is the

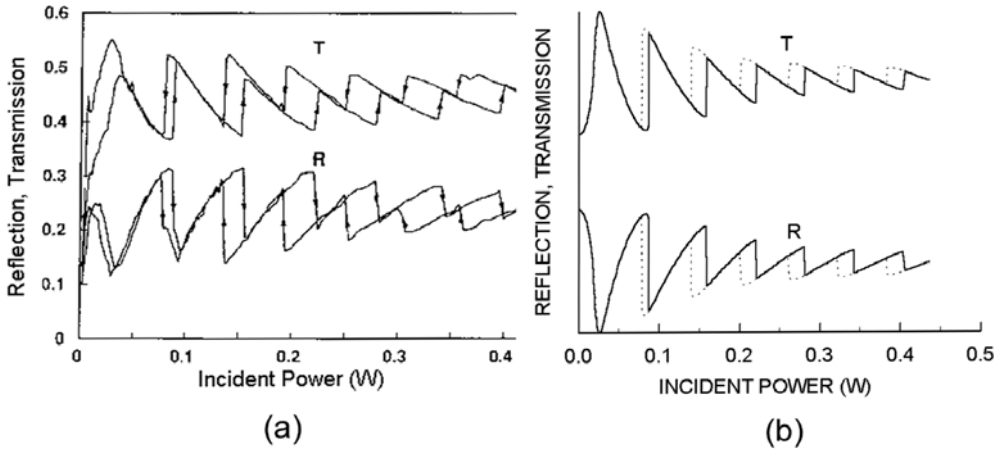

Figure 13. (a) Bistability in transmission and reflection coefficients versus incident power in 0.43 mm PMN ceramic (Chen and Scott 1993a, b). (b) Transmission and reflection resulting from the temperature curve in figure 5(b).

amplitude transmission coefficient for light leaving the sample, solution of equations (2.10) and (2.11) under the conditions described in section 3 gives the power transmitted by the sample:

$$P_T = P\{2\alpha(1-R)/\alpha_a\pi(\mathrm{e}^{\alpha L}-1)(1+R\,\mathrm{e}^{-\alpha L})\}\int_0^\infty \mathrm{d}u\,u\exp(-2u^2)A(u,\infty). \tag{4.3}$$

The integral on the right-hand side of equation (4.3) is an oscillating function of $T(0,\infty)$ with local maxima and minima at the same values of $T(0,\infty)$ as on the right-hand side of equation (4.2). Furthermore, since $\mu u \ll 1$ for $u < 2$, $K_0(\mu u)$ varies logarithmically with u across the window defined by $u\exp(-2u^2)$ (Abramowitz and Stegun 1964) and therefore equations (4.2) and (4.3) imply that $T(0,\infty)$ is approximately proportional to P_T:

$$T(0,\infty) \approx P_T K_0(\mu/2)\alpha_a(\mathrm{e}^{\alpha L}-1)(1+R\,\mathrm{e}^{-\alpha L})/\alpha(1-R)LK. \tag{4.4}$$

Hence the theoretical bistability plot for $T(0,\infty)$ closely matches the experimental bistability curve for transmitted power in ceramic PMN (Chen and Scott 1993b), reproduced in figure 5(a). Substituting for $T(0,\infty)$ from equation (4.4) into equation (4.2) gives a close match to the experimental hysteresis curves for the transmission coefficient P_T/P and the reflection coefficient $(1-P_T/P)$, as shown for ceramic PMN in figure 13. In the case of PLZT, equation (4.1) predicts multistability, which is confirmed experimentally as shown in figure 14. In the plane wave case, bistability leads to hysteresis and jumps in the transmitted and reflected beam intensities as the incident power is slowly ramped up or down, but the bistability is purely longitudinal. In the case of an incident Gaussian beam, thermo-optic bistability due to Fabry–Pérot resonance also gives rise to transverse optical bistability in the transmitted and reflected beams as observed by Chen and Scott (1993b) (see section 5 below). Relaxation oscillations in the transmitted and reflected beam intensities are observed in PMN and PLZT where the coefficient of finesse is of order 1, but not in Ce: SBN where $F_\alpha < 10^{-4}$ nor in BNN where the phase shift varies rapidly with u.

The relationship of the aperiodic temperature jumps following laser switch-on to the longitudinal bistability of the Fabry–Pérot cavity can be shown qualitatively as follows. The function $T(0,\tau)$ defined by equation (3.13) depends on its values at times earlier than τ via the function $A\{T(0,\tau')\}$. However the integrand decays to zero as τ' increases. Since

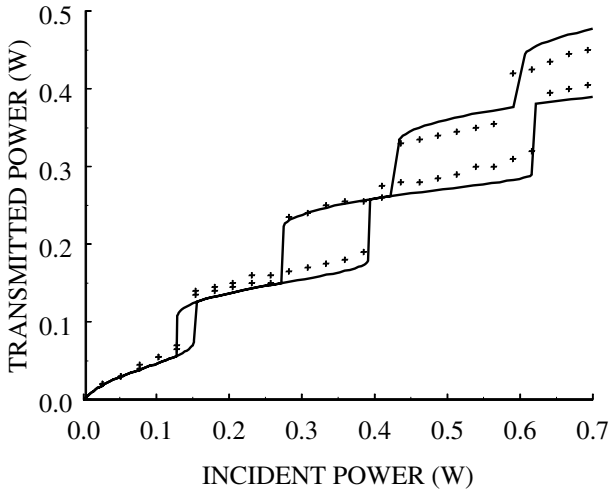

Figure 14. Bistability curve of transmitted power versus incident power in a 0.32 mm thick PLZT sample with a beam diameter of 40 μm and $\lambda = 514$ nm. Experimental data points are matched by the theoretical curve calculated using equation (4.2).

$A\{T(0,\tau')\} \approx A_s$ except during jumps of duration $\Delta\tau \approx 1$, we approximate the right-hand side of equation (3.13) by replacing $A\{T(0,\tau')\}$ by $A\{T(0,\tau)\}$ on $0 \leqslant \tau' < \Delta\tau$ and by A_s on $\Delta\tau \leqslant \tau' < \infty$, which gives

$$T(0,\tau) \approx \frac{2P}{\pi LK}\left\{A(0,\tau)\int_0^{\Delta\tau}\frac{\mathrm{d}\tau'}{1+8\tau'}\exp(-\mu^2\tau') + A_s\int_{\Delta\tau}^{\tau}\frac{\mathrm{d}\tau'}{1+8\tau'}\exp(-\mu^2\tau')\right\}$$

i.e.

$$T(0,\tau) \approx T_s(0,\tau) + [\{A(0,\tau)/A_s\} - 1]T_s(0,\Delta\tau).$$

Hence

$$\{T(0,\tau) - T_s(0,\tau) + \Delta_1\}[1 + F_\alpha \sin^2\{kL(n_0 + T(0,\tau)\,\mathrm{d}n/\mathrm{d}T)\}] = \Delta_2 \quad (4.5)$$

with

$$\Delta_1 = A_{max}P\ln(1+8\Delta\tau)/4\pi LK$$

and

$$\Delta_2 = A_s P\ln(1+8\Delta\tau)/4\pi LK$$

where we have used the small argument approximation $E_1(x) \sim -\ln x - \gamma'$ (where $\gamma' =$ Euler's constant) in equation (3.2) since $t_K/8t_c = w^2H/4LK$ is of order 10^{-5}.

Graphical solution of equation (4.5) gives a multi-branched bistability curve for $T(0,\tau)$ bounded by the curves $T_s(0,\tau) + \Delta_2 - \Delta_1$ and $T_s(0,\tau) + \Delta_2/(1+F) - \Delta_1$ with aperiodic thermal switches between branches as shown in figure 15. Since $T(0,\tau)$ has an upper bound, there is a finite number of thermal switches which occur at increasing time intervals.

4.2. Switching times for thermo-optic bistability

Equation (3.2) gives an analytic expression for the smoothed axial temperature $T_{sm}(0,\tau)$. Comparison with either the finite element solution or the integral equation solution of

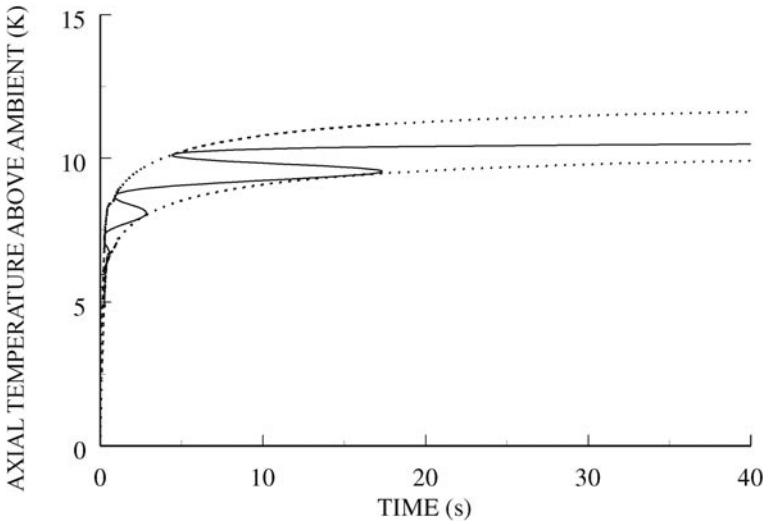

Figure 15. Bistability curve of T versus t from equation (4.5). The upper and lower envelopes are given in the text.

equations (3.10) and (3.12) shows that $T_{sm}(0, \tau)$ differs by $\pi/(kL\,\mathrm{d}n/\mathrm{d}T)$ at adjacent thermal switches which occur at the maxima of $A\{T(0, \tau)\}$ (e.g. see figure 12(b)). Hence, to within an additive uncertainty given by the initial detuning, the switching times τ_m are given by

$$T_{sm,m}(0, t) = \frac{m\pi}{kL\,\mathrm{d}n/\mathrm{d}T} = \frac{A_s P}{4\pi LK} \exp\left(\frac{t_K}{8t_c}\right)\left[E_1\left(\frac{t_K}{8t_c}\right) - E_1\left\{\frac{t_K}{8t_c}(1 + 8\tau_m)\right\}\right] \quad \text{for } m = 1, 2, 3, \ldots. \tag{4.6}$$

Since $E_1(x) \to 0$ as $x \to \infty$ there is a finite number M of thermal switches given by

$$\frac{M\pi}{k\,\mathrm{d}n/\mathrm{d}T} = \frac{A_s P}{4\pi K} \exp\left(\frac{t_K}{8t_c}\right) E_1\left(\frac{t_K}{8t_c}\right) \approx -\frac{A_s P}{4\pi K}\left[\ln\left(\frac{w^2 H}{4LK}\right) + \gamma'\right] \tag{4.7}$$

where we have used the small argument approximation for $E_1(x)$. Using the same approximation, equation (4.6) remains a transcendental equation for τ_m in general:

$$\frac{m\pi}{k\,\mathrm{d}n/\mathrm{d}T} = -\frac{A_s P}{4\pi K}\left[\ln\left(\frac{t_K}{8t_c}\right) + \gamma' + E_1\left\{\frac{t_K}{8t_c}(1 + 8\tau_m)\right\}\right]. \tag{4.8}$$

Since equation (4.6) is based on the infinite disc solution, the value of M given by equation (4.7) must be corrected in accordance with figure 9(b) for samples of radius <6 mm. Note that τ_m is insensitive to the value of H for the early jumps, but the timing of the later jumps is highly sensitive to the flow velocity of the atmosphere surrounding the sample via the H-dependence of t_c. This is important for the sensing application described by Scott and Chen (1992).

Equation (4.8) can be compared with the empirical formula for the switching times in ceramic PMN reported by Scott and Chen (1992). In the present notation, they found that t_m for the last few switching events could be fitted to the formula

$$t_m = t_n P/\{P - (m - n)P_0\} \tag{4.9}$$

where t_n is the time of the first switching event observed on the macroscopic timescale and $P_0 =$ constant. Equation (4.9) follows from equation (4.8) under the approximation $E_1(x) \approx 1/4x$ in the range $0.1 < x < 1$. A more accurate rational approximation $E_1(x) \approx 0.33/(x + 0.075)$

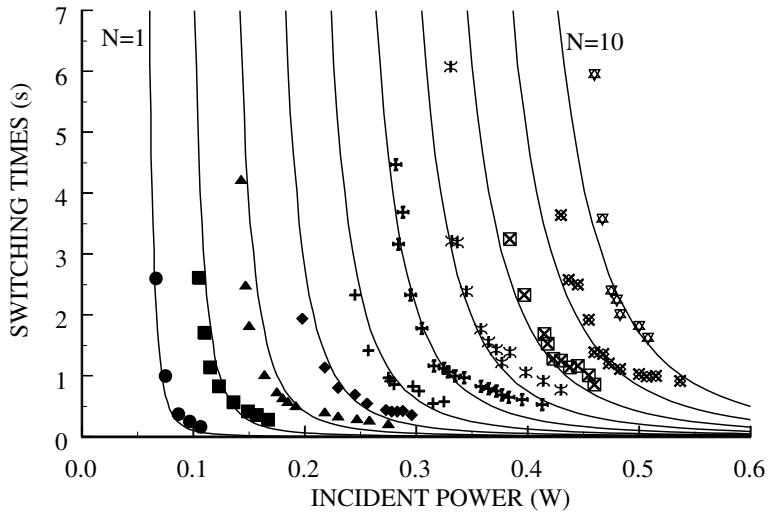

Figure 16. Aperiodic switching times in PMN. The data points are the times from laser switch-on for experimental switching events in 0.43 mm ceramic PMN for indicated values of incident laser power given in Chen *et al* (1992). The theoretical curves are given by equation (4.6) for the experimental parameter values. N = switching event number.

for $0.01 < x < 0.3$ gives the empirical formula $t_m = \{A_1(P) + mA_2\}/(P - mP_0)$, which was fitted to the experimental switching times plotted by Chen *et al* (1992). Hence their empirical fitting parameters are related to the experimental parameters as follows:

$$P_0 = \frac{2\pi\lambda K}{A_s\,\mathrm{d}n/\mathrm{d}T}\left\{\exp\left(\frac{w^2H}{4LK}\right)E_1\left(\frac{w^2H}{4LK}\right)\right\}^{-1} \qquad A_2 = \frac{0.075\rho cL}{2H}P_0$$

$$A_1(P) = \frac{\rho cL}{2H}\left[0.33\left\{\exp\left(\frac{w^2H}{4LK}\right)E_1\left(\frac{w^2H}{4LK}\right)\right\}^{-1} - 0.075\right]P. \tag{4.10}$$

Figure 16 compares the switching times given by equation (4.8) and the experimental data shown in figure 7 of Scott and Chen (1992). In both that figure and figure 16, there is a zero shift of 20 mW in incident power, due to a combination of initial detuning and stray light. It is known that K varies with temperature in the vicinity of the ferroelectric phase transition for the perovskites lead titanate and barium titanate (Mante and Volger 1967, Yoshida 1960) but no data have been published on $K(T)$ for PMN or PLZT. In PMN $\mathrm{d}n/\mathrm{d}T$ is approximately constant over the experimental temperature range (Korshunov *et al* 1992). Figure 16 shows a close fit between experimental switching times and our constant K model for incident power below about 300 mW, but at higher power the experimental switching times for the highest values of m are delayed relative to the predictions of this model. This is consistent with a dip in the $K(T)$ curve at higher temperature (30–40 degrees above ambient), which causes reduced cooling and hence greater curvature in the central region of the smoothed plot of temperature against time. Hence we conclude that for ceramic PMN, $K(T)$ goes through a local minimum at the phase transition as in related ferroelectrics (Nettleton 1970). Furthermore this suggests a new optical method for measuring the temperature dependence of thermal conductivity in the vicinity of a phase transition, distinct from the method of Burkhart and Rice (1977).

5. Transmitted and reflected beam patterns

Although the zeroth order expression for I_c given by equation (3.4) is sufficiently accurate to determine the azimuthally averaged temperature profile, as well as the temporal variation of the total transmitted power, it does not contain sufficient information on the phase and amplitude variation of the intracavity beam to determine the radial profile of the transmitted and reflected beams in the near or far field. In order to determine these, we must obtain the first order iterative solution for the light fields of the forward and backward travelling waves within the resonator by solving equations (2.10) and (2.11) using the zeroth order solution for the temperature profile given by equations (3.10) or (3.12).

In the steady state, analytical expressions for the near and far field radial irradiance distribution of the transmitted and reflected beam patterns can be obtained by solving equations (2.10) and (2.11) using the steady state temperature profile in the nonlinear phase terms $ik\{n_0 + (dn/dT)T(u,\tau)\}$. In the region of the beamwidth, it follows from equation (3.6) that the radial dependence of the temperature profile is independent of the disc radius as follows.

For $u \leqslant 2$, $\mu u \leqslant 0.02$ and hence we can use the ascending series approximations (Abramowitz and Stegun 1964): $I_0(x) \sim 1 + x^2/4 + \cdots$ and $K_0(x) \sim -\{\ln(x/2) + \gamma'\}I_0(x) + x^2/4 + \cdots$ in equation (3.6) to obtain $T(u) \sim T(0)I_0(\mu u) + (2A_sP/\pi w^2 LK)\int_0^u du'\, u' \ln(u'/u)\exp(-2u'^2)$.

Integration by parts gives

$$T(u) \sim T(0)I_0(\mu u) + (A_sP/2\pi LK)\int_0^u du'\,\{1 - \exp(-2u'^2)\}/u'$$

Hence $T(u) \sim T(0)(1 + \mu^2u^2/4) - A_sP\,\mathrm{Ein}(2u^2)/4\pi LK$ where $\mathrm{Ein}(x) \equiv \ln x + \gamma' + E_1(x)$ (Abramowitz and Stegun 1964). $\mathrm{Ein}(x)$ has the ascending series $\sum_{n=1}^{\infty}(-1)^{n+1}x^n/nn!$ and, for typical experimental parameters, $A_sP/2\pi LKw^2$ is four orders of magnitude greater than $\mu^2T(0)/4$ so that $T(u)$ has the parabolic approximation:

$$T(u) \sim T(0) - A_sPu^2/2\pi LK \qquad \text{for } u \leqslant 0.5.$$

Although $T(0)$ depends on the disc radius, the temperature gradient is independent of disc radius for $u \leqslant 0.5$.

To solve equations (2.10) and (2.11) in the 'paraxial approximation' $u^2 \ll 1$, with the parabolic approximation for $T(u)$, we use the eikonal ansatz (Ghatak and Thyagarajan 1978, following Akhmanov *et al* 1968b):

$$E(u,\zeta) = E_0(u,\zeta)\exp\{ikn_0\zeta + ikn_0S(u,\zeta) - \alpha\zeta/2\}L$$
$$\text{with} \qquad S(u,\zeta) = u^2\beta(\zeta)/2 + \phi(\zeta) \tag{5.1}$$

which must satisfy equation (2.10) on the interval $0 \leqslant \zeta < \infty$ with the boundary condition $E(u,0) = \mathcal{T}E_i(u,0)$. $E_F(u,\zeta)$ and $E_B(u,\zeta)$ are obtained from $E(u,\zeta)$ by means of a multiple beam expansion as in the case of an incident plane wave:

$$E_F(u,\varsigma) = \sum_{j=1}^{\infty} E_{Fj}(u,\varsigma) \qquad \text{and} \qquad E_B(u,\varsigma) = \sum_{j=1}^{\infty} E_{Bj}(u,\varsigma)$$

where $E_{Fj}(u,\varsigma) = R^{j-1}E(u,2j-2+\varsigma)$ and $E_{Bj}(u,\varsigma) = R^{j-1/2}E(u,2j-\varsigma)$ for $j = 1, 2, 3, \ldots$.

The transmitted and reflected beams are therefore given by

$$E_T(u) = \mathcal{T}'\sum_{j=1}^{\infty} R^{j-1}E(u,2j-1) \tag{5.2}$$

$$E_R(u) = -\sqrt{R}E_i(u) + \mathcal{T}' \sum_{j=1}^{\infty} R^{j-1/2} E(u, 2j) \tag{5.3}$$

where $\mathcal{T}'$ is the amplitude transmission coefficient for light leaving the sample. In the case of negligible finesse, only the first terms on the right-hand side of equations (5.2) and (5.3) are required.

Substituting the ansatz (5.1) into equation (2.10) gives

$$\begin{aligned} &E_0(u, \varsigma) = E_p \exp\{-u^2/f^2(\varsigma)\}/f(\varsigma) \qquad \beta(\zeta) = w^2 f'(\zeta)/L^2 f(\zeta) \\ &\phi'(\zeta) = T(0)(\mathrm{d}n/\mathrm{d}T)/n_0 - 1/\{2k^2 n_0^2 w^2 f^2(\varsigma)\} \end{aligned} \tag{5.4}$$

where

$$2f^2(\varsigma) = 1 + (QG)^{-1} + \{1 - (QG)^{-1}\}\cos(2L\sqrt{G}\varsigma) \tag{5.5}$$

$Q = 4k^2 n_0^2 w^4$, $G = A_s P(\mathrm{d}n/\mathrm{d}T)/\pi w^2 LKn_0$ and E_p is the amplitude of the incident beam at $u = 0$. This result differs from that of Ghatak and Thyagarajan in two ways. Firstly we have used the temperature profile averaged over sample thickness rather than $T(u, \zeta)$. Secondly they obtain the solution for $f(\zeta)$ in the defocusing case, in which oscillation of the beam radius does not occur; in the thermal focusing case, however, equation (5.5) shows that the effective beamwidth of the forward beam oscillates periodically in z as first pointed out by Wagner *et al* (1968). The self-trapping condition, under which self-focusing just balances diffraction, is given by $QG = 1$, which gives the critical power for self-trapping as $P_c = \pi LK/4k^2 w^2 A_s n_0(\mathrm{d}n/\mathrm{d}T)$. For the parameter values of our PMN experiments, $QG \approx 10^2 \gg 1$ so thermal focusing dominates over diffraction. The beamwidth decreases from the incident value w to its first minimum (with beamwidth $w/\sqrt{QG}$) at $z = \pi/2\sqrt{G} = 2.2$ mm. For a sample thickness of $L = 0.74$ mm, the beamwidth at the rear face is $0.86w$.

Although the parabolic phase ansatz in equation (5.1) is reasonable in the paraxial approximation, we show below that it significantly overestimates the phase variation for $u \geqslant 0.5$ and hence is unsuitable for determining the radial dependence of the far field transmitted beam pattern in the case of thermo-optic nonlinearity. To obtain a better approximation for the radial phase profile of the intracavity beam, we need a more physically realistic phase ansatz. Since the phase of the beam is determined, according to equation (2.4), by $n(u) = n_0(1 + \chi T(u))$, an appropriate phase ansatz is the function $\mathrm{Ein}(2u^2)$, which accurately describes the temperature profile for $u \leqslant 2$. In appendix B we solve equation (2.10) using the ansatz

$$S(u, \zeta) = \beta(\zeta)\mathrm{Ein}(2u^2) + \phi(\zeta) \tag{5.6}$$

to obtain the result $\beta(\zeta) = -w^2 g'(\zeta)/8L^2$, $\phi'(\zeta) = 2\{1-2\,\mathrm{e}^{g(\varsigma)}\}/k^2 n_0^2 w^2 + T(0)(\mathrm{d}n/\mathrm{d}T)/n_0$, and hence

$$E_0(u, \varsigma) = E_P \exp\tfrac{1}{2}\{-g(\varsigma) - 2u^2\}/[1 + \{\mathrm{e}^{-g(\varsigma)} - 1\}\exp(-2u^2)] \tag{5.7}$$

where $g(\zeta)$ satisfies the equation

$$g'^2(\varsigma) = \frac{4A_\infty PL}{\pi Kn_0 w^2}\frac{\mathrm{d}n}{\mathrm{d}T}g(\varsigma) - \frac{16L^2\{g(\varsigma) - 12\,\mathrm{e}^{g(\varsigma)} + 6\,\mathrm{e}^{2g(\varsigma)} + 6\}}{k^2 n_0^2 w^4}. \tag{5.8}$$

Equation (5.8) is the equation of a nonlinear oscillator with 'kinetic energy' $g'^2(\varsigma)$, 'total energy' $W = -96L^2/k^2 n_0^2 w^4$, 'potential energy' $V(g) = 16L^2(g - 12\,\mathrm{e}^g + 6\,\mathrm{e}^{2g})/k^2 n_0^2 w^4 - 4A_\infty PLg(\mathrm{d}n/\mathrm{d}T)/\pi LKn_0 w^2$ and the initial conditions $g(0) = 0 = g'(0)$. Putting $V'(g) = 0$ shows that $V(g)$ has a single real minimum at $g = \ln[\frac{1}{2}\{1 + \sqrt{\frac{2}{3}(1 + n_0 k^2 w^2 A_\infty P(\mathrm{d}n/\mathrm{d}T)/8\pi LK)}\}]$. Hence $g(\zeta)$ oscillates between 0 and its maximum

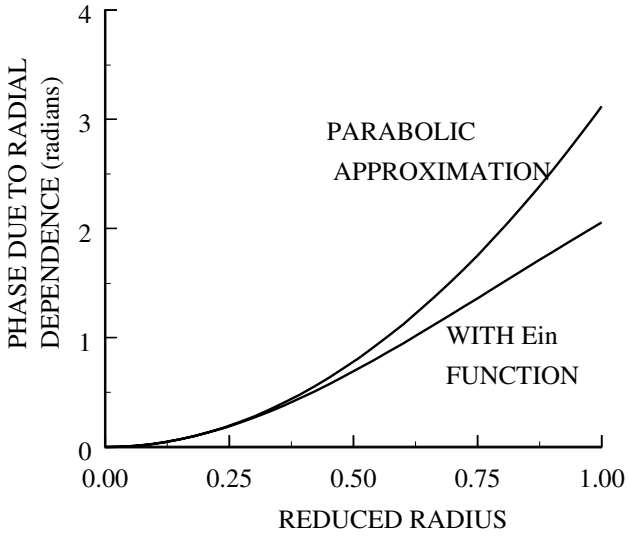

Figure 17. Comparison of the phase factor $\mathrm{Ein}(2r^2/w^2)$ with the parabolic (paraxial) approximation.

value g_{max} (given by $V(g) = W$) as ζ increases. Therefore the amplitude and phase terms given in equations (5.6) to (5.8) also oscillate periodically in ζ, as in the paraxial approximation (equations (5.4) and (5.5)). Solving equation (5.8) numerically and substituting for $g(\zeta)$ in equation (5.7) shows that, for the parameter values of our experiments, the amplitude and beamwidth deviate only slightly from those given by the paraxial approximation but the radial phase factor in equation (5.6) is significantly less steep than the parabolic factor in equation (5.1) in the range $0.5 \leqslant u \leqslant 2$, reflecting the decrease in slope of the temperature profile in that region (see figure 17).

In both the paraxial approximation and the $\mathrm{Ein}(2u^2)$ approximation, the beamwidth of the first transmitted beam decreases by only 10–15% across typical PMN and PLZT samples and equations (3.6) and (3.12) show that the central temperature is only a logarithmic function of beamwidth, being approximately proportional to absorbed power irrespective of beamwidth. Hence the assumption of a cylindrical Gaussian heat source in section 3 is self-consistent.

Substituting equations (5.6)–(5.8) into equations (5.2) and (5.3) gives the amplitude and phase of the transmitted and reflected beams in the near field. By computing the squared modulus of the Fourier transform of these patterns, we obtain the theoretical transmitted and reflected far field irradiance patterns, which closely match the experimental ones. For example figure 18 compares the experimental and calculated far field steady state irradiance patterns for the beam transmitted from a PMN sample of thickness 1.4 mm with incident beamwidth of 78 μm and given values of incident beam power, showing the same number of rings and angular diameter in the experimental and theoretical patterns. Since $R = 0.20$ for PMN, the series (5.2) and (5.3) converge rapidly as shown by figure 18. It should be noted that, although the Fabry–Pérot effect is responsible for the thermo-optic bistability which causes the aperiodic jumps in beam profiles, the primary ring patterns in those profiles are caused by the temperature-induced radial phase variation of the first-pass beams $E_{F1}(u, \zeta)$ and $E_{B1}(u, \zeta)$ (i.e. they are due to thermal focusing) rather than by Fabry–Pérot interference.

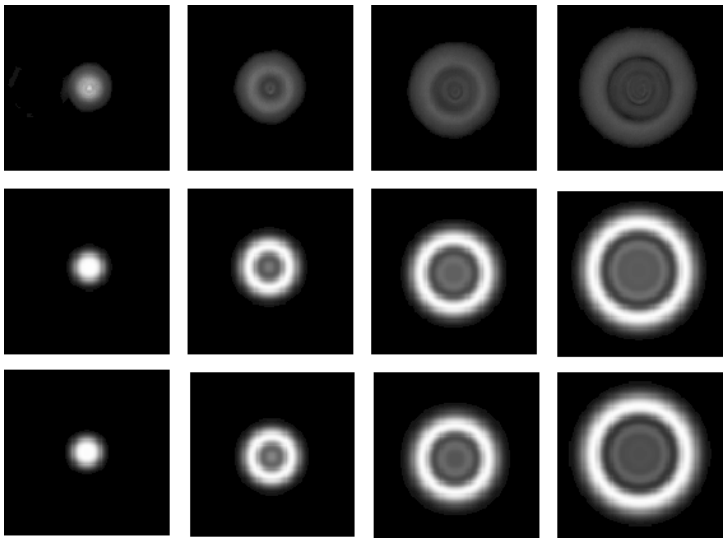

Figure 18. Far field beam patterns transmitted by a 1.4 mm PMN crystal illuminated via a 40 cm focal length lens; experimental photographs in top row, theoretical plots in middle and bottom rows. The middle row contains patterns produced by the first pass through the crystal; the bottom row shows the patterns after five passes through the crystal. Incident power from left to right: 100 mW, 200 mW, 300 mW and 400 mW.

For radial symmetry, the full spatio-temporal variation of the light fields for a thin sample, following rapid laser switch-on, can be obtained by numerical solution of equations (2.10) and (2.11) with the appropriate time-dependent temperature profile. For materials with negligible bistability, such as Ce:SBN and BNN, we use equation (3.1) and for bistable materials with finesse of order 1, such as PLZT and PMN, we use equation (3.10) or (3.12) or the finite element solution of equations (3.3) and (3.5) shown in figure 9(a).

Figure 2 shows experimental plots of central and total transmitted intensity from a PMN sample, compared with plots computed using equation (5.7) for the amplitude and equation (3.12) for the time dependent phase factor of the near field transmitted beam. Figure 3 shows experimental plots of central intensity transmitted from a Ce:SBN ceramic sample, compared with plots computed using equation (5.7) for the amplitude of and equation (3.1) for the time dependent phase factor.

The main features of the evolution of the light fields towards their steady state radial patterns can be understood from the fact that, after a brief initial transient phase, i.e. for $t_c \gg t \gg t_K$, $T(u, \tau)$ evolves through a sequence of quasi-stationary states separated by rapid jumps. Examination of the plots of $T(u, \tau)$ in figures 9(a) and 12(a) shows a characteristic cyclic variation of the temperature gradient within the region of the laser beam (for say $u < 2$), superimposed on the overall gradual relaxation of the temperature to its steady state profile (see figure 19).

(i) Between jumps the axial absorption factor $A(0, \tau)$ is near its minimum A_{min}, $\partial T/\partial \tau \approx 0$ and $2HT(0, \tau) < 2HT_{st}(0)$ is more than three orders of magnitude smaller than $I_{abs}(0)$ in typical experiments. Hence according to equation (3.3) $T(u, \tau)$ is a metastable temperature profile approximately equal to the steady state profile scaled by a factor $T(0, \tau)/T_{st}(0)$ and the power of the thermal lens is given by the central curvature of the temperature profile: $\nabla_u^2 T(0, \tau) = 2\partial^2 T(0, \tau)/\partial u^2 \approx -2PA_{min}/\pi LK$.

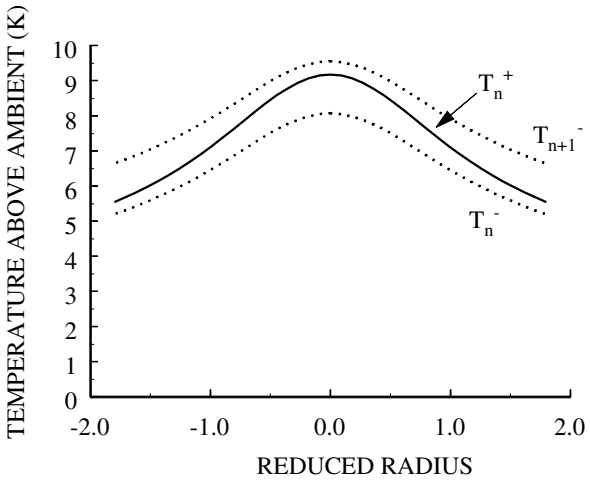

Figure 19. Radial temperature profiles just prior to a jump, $T(r, t_n^-)$, immediately after a jump, $T(r, t_n^+)$, and immediately prior to the next jump $T(r, t_{n+1}^-)$, given by equation (3.12). (At 2 s, 2.5 s and 5 s in figure 12(b)).

(ii) At a jump the axial absorption factor goes rapidly through its maximum A_{max} as $\partial T/\partial\tau(0,\tau)$ goes through its maximum $\approx\Delta T/(\tau = 1) = \pi/kL\,\mathrm{d}n/\mathrm{d}T$. Hence the magnitude of the central curvature goes through a maximum given by $\{2PA_{max}/\pi K - \pi/k(\mathrm{d}n/\mathrm{d}T)\}/L$, which is typically between one and two times $2PA_{min}/\pi LK$. This causes an outward jump in the diameter of the far field beam pattern corresponding to the jumps in central and total transmitted power.

We can compute the transmitted beam pattern before each jump from equations (5.6) to (5.8). The near field beam pattern immediately after each jump has a slightly larger peak amplitude and steeper phase profile than before and hence the far field ring pattern will have a larger diameter. As $T(u,\tau)$ relaxes to the metastable profile, the phase profile becomes less steep and hence the diameter of the far field pattern relaxes back to the diameter before the previous jump. This explains the quasi-cyclic pattern of rapid outward jumps followed by slow inward relaxation of the diameter of the observed far field beam patterns.

6. Discussion and conclusions

Transient oscillations under steady illumination, such as those in BNN and Ce:SBN, do not necessarily indicate optical bistability. True optical bistability involves the existence of multiple *stable* output states for a single value of incident power above some threshold, as shown in PMN in figure 5. As we have shown, it arises in PMN and PLZT from thermal bistability due to Fabry–Pérot feedback and involves a theoretical S-shaped dependence of temperature on incident power and on time. In transient observations, it is indicated by an aperiodic sequence of relaxations towards metastable output values as in figure 2.

The steady state optical bistability curves as well as the occurrence and timing of aperiodic relaxation oscillations in PMN and PLZT can be explained quantitatively by a diffusive nonlinear etalon model in which the sample thickness is less than the waist length of the incident laser beam. We have shown that the optical bistability observed arises from *longitudinal*

bistability in the axially averaged temperature profile and that the jumps in the transmitted beam patterns correspond to jumps in the temperature profile over the beam width ('whole beam switching'). Switching waves outside the beam width do not occur. The radially symmetric *transverse* oscillations observed in the far field transmitted and reflected beams are a consequence of relaxation oscillations in the refractive index profile driven by oscillations in the mean internal beam intensity. In order to model these transverse effects, including the correct form for the curve of central irradiance against time (figure 2), the temperature profile from section 3 was substituted into equations (2.10) and (2.11), which were then solved in the first iteration (including the ∇_u^2 terms) to determine the phase and amplitude of $E_F(u, \zeta)$ and $E_B(u, \zeta)$ and to verify the initial assumption of z independence of the heating term.

As shown in figure 18, the computed far field transmitted beam patterns closely match those produced by a 1.4 mm thick PMN sample for the stated values of beamwidth and power. For combinations of beamwidth, laser power and sample thickness which produce a somewhat greater maximum local irradiance within the sample, the circular symmetry in the centre of the pattern is broken and the central rings of the thermal focusing patterns are replaced by high contrast patterns which may have lower symmetry. Both hexagonal and chaotic patterns have been observed in the central region of the beam patterns produced by PMN (Scott and O'Sullivan 1996, Scott *et al* 1996) and a diamond pattern is observed in BNN (Chen and Scott 1993a). In section 3, we have shown that the temperature variation in the z direction in ferroelectric samples subjected to c.w. laser illumination in experiments reported to date is of the order of 1% or less. Hence the radially symmetric bistability phenomena so far observed can be quantitatively explained in terms of a temperature profile which depends only on r and t. Nevertheless, if the spatial symmetry breaking observed in BNN and PMN is due to thermo-optic effects, z dependence must be taken into account in order to calculate the magnitude of the thermal diffraction grating produced in the sample. For Gaussian illumination, the thermal grating vector will have a radial component which varies with position in the sample. For each value of the grating vector, the diffraction it produces will tend either to reinforce or to suppress it, resulting in either positive or negative feedback as shown by Firth (1990). In future work, we will investigate whether the non-planar generalization of this grating is able to account for the observed radial symmetry breaking or whether another effect in addition to the thermo-optic effect (e.g. the photo-refractive effect) is involved.

One should note that aperiodic relaxation oscillations do not require oscillation in temperature (Rozanov 1981) in any part of the sample and such temperature oscillations have not been observed experimentally in PMN to date. Sequences of aperiodic oscillations which appear to approach a periodic regime as the phase transition is approached have been observed by Chen and Scott (1993b). However, experiments to date have not shown the existence of perfectly periodic oscillations, unlike other optical bistability systems (including liquid crystals, atomic vapours and semiconductors). Thus the existence of a periodic oscillation threshold in parameter space remains an open question and, in our judgment, an important one. In a separate paper we show the existence of a threshold for Hopf bifurcation to a regime of periodic oscillations and shown that it lies not far above the power density limits used in experiments to date. Thus future experiments should endeavour to use higher power levels (subject to optical damage thresholds) very near T_C (where $\mathrm{d}n/\mathrm{d}T$ is maximum) in order to search for this predicted threshold. In a diffusively nonlinear thermo-optic Fabry–Pérot resonator with thickness less than a few mm, the thermal conduction time t_K is many orders of magnitude greater than the round-trip time t_R of the light. The minimum value of t_K given by $w \rightarrow \lambda$ is about 1 μs, whereas $t_R < 70$ ps for samples <1 cm thick. Hence *periodic oscillations* in the light output from such a system would be quite different in origin from the periodic oscillations described by Ikeda *et al* (Ikeda 1979, Ikeda *et al* 1980) and Goldstone

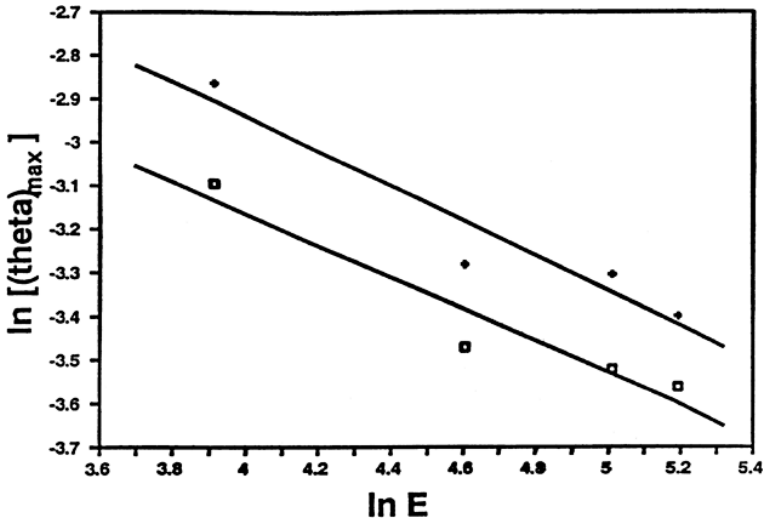

Figure 20. Beam deviation angle against applied field electric field at the transition temperature in BNN, with slope $-2/\delta$ where δ is the critical exponent characterizing the response electric displacement to field along the critical isotherm. The data points are for the c axis (top) and the a axis (bottom) and the lines correspond to $\delta = 5$ (Chen and Scott 1992).

and Garmire (1981), in which the optical round-trip time is comparable to the response time of the medium (see also Cheung *et al* 1983 and Khoo *et al* 1984). In that case, of course, the SVEA equations must include time derivatives.

Truly periodic oscillations can also occur in thermo-optic materials in which other processes additional to heat flow occur, provided their timescales are comparable to the thermal diffusion time t_K. This is not the case in the photorefractive process in PMN but it can be realized in liquids in which the absorbing species is subject to diffusion or in which phase changes occur.

For relaxor ferroelectrics such as PMN and PLZT, one can approximate $\mathrm{d}n/\mathrm{d}T =$ constant below or above the phase transition temperature. However, in most crystals with displacive phase transitions, $n(T)$ varies as $(T_0 - T)^\beta$ over a range from 1 to 20 K below the transition, where $\beta = 1/2$ for second-order transitions and 1/4 near tricritical points. This is true at both magnetic phase transitions and structural phase transitions (Becker and Gehring 1975, Gehring 1976, Harley and Macfarlane 1975). Note that thermal focusing, with focal strength directly proportional to $\mathrm{d}n/\mathrm{d}T$, is a more sensitive measurement of critical indices than is birefringence, which is proportional to $n(T)$. The divergence in $n(T)$ can be very large and is probably greatest in tetragonal–cubic transformation in the ferroelastic scheelite $BiVO_4$. In that material Δn is 1.4×10^{-2} from 515 to 520 K and 2.75×10^{-2} from 505 to 515 K, so that $\mathrm{d}n/\mathrm{d}T = 2.8 \times 10^{-3}$ K^{-1} over a range of $\sim$15 K (Wood *et al* 1980). This value can be further enhanced to $\mathrm{d}n/\mathrm{d}T = 6 \times 10^{-3}$ K^{-1} by applying 0.6 GPa of hydrostatic pressure (Wood and Glazer 1980). In such systems thermal focusing should be very large; as many as 35 interference rings are observed in the far field pattern in $Ba_2NaNb_5O_{15}$ (Scott *et al* 1991, Chen *et al* 1991a). The peak value of $\mathrm{d}n/\mathrm{d}T$ just below the transition in this material is 2.5×10^{-3} (Yamada *et al* 1970).

It is also possible in ferroelectrics to increase $n(T)$ and $\mathrm{d}n/\mathrm{d}T$ near the Curie temperature by application of an electric field E (Beale *et al* 1991). Many ferroelectrics are nearly tricritical, such that their phase transitions become second order by application of modest electric fields. This has been studied in great detail for KH_2PO_4 (Courtens and Gammon 1981) and

$Ba_2NaNb_5O_{15}$. The latter tungsten bronze structure has a phase transition near 845 K that is tricritical. The electric field required to reach its second-order transition point(s) at 845 K is 0.32 ± 0.02 kV cm^{-1} (Sheih *et al* 1991), at which point they determine from thermal focusing experiments $\beta = 0.28 \pm 0.01$, $\gamma = 0.94 \pm 0.02$ and $\delta = 5.0 \pm 0.2$ (see figure 20). Under such a field its thermal focussing increases approximately 25%. In addition, a fluctuation-quenching phenomenon occurs such that the shape of the curve describing thermal focussing magnitude versus temperature changes with field. This has been interpreted not as a change in $n(T, E)$ with field, but as due to a change in thermal conductivity $K(T, E)$ with field (Scott and Sheih 1990) due to fluctuation quenching of the cusplike dip in thermal diffusion for that material (Nettleton 1970). Such large changes in $K(T, E)$ with field ($\sim$20% per kV cm^{-1}) were first reported by Sievers (1963) in strontium titanate and explained theoretically by Fatuzzo (1964), but in general neither the sign nor magnitude of $\mathrm{d}K/\mathrm{d}T$ near T_C can be predicted from theory (Nettleton 1970). As shown in section 4, for materials which exhibit aperiodic thermo-optic switching oscillations, comparison of the experimental switching times with those given by our model can be used to estimate the temperature dependence of K, including the cusplike anomaly near T_C.

Appendix A. Green function and $T(u, \zeta, \tau)$ for Gaussian heating with constant absorption factor

The heat equation in dimensionless cylindrical polar coordinates for the temperature $T(u, \zeta, \theta, \tau)$ due to an instantaneous point heat source of strength Ω at $(u', \zeta', \theta', \tau')$ is

$$\frac{\partial^2 T}{\partial u^2} + \frac{1}{u}\frac{\partial T}{\partial u} + \frac{w^2}{L^2}\frac{\partial^2 T}{\partial \varsigma^2} + \frac{1}{u^2}\frac{\partial^2 T}{\partial \theta^2} - \frac{\partial T}{\partial \tau} = -\Omega\delta(\vec{u} - \vec{u}')\delta(\tau - \tau') \qquad \text{(A.1)}$$

where $u = r/w$, $\zeta = z/L$, $\tau = \kappa t/w^2$, $\kappa = K/\rho c$ = thermal diffusivity, L = sample thickness, K = thermal conductivity, w = beamwidth, ρ = density and c = specific heat.

The solution for the region $0 \leqslant \zeta \leqslant 1$ with the 'radiation boundary condition' $\partial T/\partial \zeta = \pm hT$ at the faces $\zeta = 0, 1$ and $\tau' = 0$ is Ω times the Green function given in Carslaw and Jaeger (1959) for a unit source:

$$T = \frac{\Omega\, \mathrm{e}^{-U^2/4\tau}}{2\pi\tau} \sum_{n=1}^{\infty} \frac{g_n(\varsigma) g_n(\varsigma')}{(\gamma_n^2 + h^2) + 2h}\, \mathrm{e}^{-(\gamma_n w/L)^2 \tau}$$

where $g_n(\varsigma) = (\gamma_n \cos \gamma_n \varsigma + h \sin \gamma_n \varsigma)$, $U^2 = u^2 + u'^2 - 2uu' \cos(\theta - \theta')$, $h = HL/K$, H = sum of linearized convection and radiation coefficients and γ_n (for $n = 1, 2, 3, \ldots$) are the roots of the equation

$$\tan \gamma = 2\gamma h/(\gamma^2 - h^2). \qquad \text{(A.2)}$$

Changing the axial variables to $\bar{\varsigma} = \varsigma - 1/2$ and $\bar{\varsigma}' = \varsigma' - 1/2$, we obtain

$$g_n(\varsigma) = (\gamma_n \cos \gamma_n/2 + h \sin \gamma_n/2) \cos \gamma_n \bar{\varsigma} + (h \cos \gamma_n/2 - \gamma_n \sin \gamma_n/2) \sin \gamma_n \bar{\varsigma}.$$

Hence

$$\begin{aligned} g_n(\varsigma) g_n(\varsigma') = {} & B_n \cos \gamma_n \bar{\varsigma} \cos \gamma_n \bar{\varsigma}' + C_n \sin \gamma_n \bar{\varsigma} \sin \gamma_n \bar{\varsigma}' \\ & + D_n(\cos \gamma_n \bar{\varsigma} \sin \gamma_n \bar{\varsigma}' + \sin \gamma_n \bar{\varsigma} \cos \gamma_n \bar{\varsigma}') \end{aligned}$$

where

$$\begin{aligned} D_n = {} & (\gamma_n \cos \gamma_n/2 + h \sin \gamma_n/2)(h \cos \gamma_n/2 - \gamma_n \sin \gamma_n/2) = \gamma_n h(\cos^2 \gamma_n/2 - \sin^2 \gamma_n/2) \\ & + (h^2 - \gamma_n^2) \sin \gamma_n/2 \cos \gamma_n/2 = 0 \end{aligned}$$

by equation (A.2)

$$\begin{aligned} B_n &= (\gamma_n \cos \gamma_n/2 + h \sin \gamma_n/2)^2 = (\gamma_n + h \tan \gamma_n/2)^2 \cos^2 \gamma_n/2 \\ C_n &= (h \cos \gamma_n/2 - \gamma_n \sin \gamma_n/2)^2 = (h - \gamma_n \tan \gamma_n/2)^2 \cos^2 \gamma_n/2. \end{aligned}$$

Since $\tan\gamma = 2(\tan\gamma/2)/(1-\tan^2\gamma/2)$, there are two branches of solutions for $\tan\gamma/2$ arising from equation (A.2). For $n = 1, 3, 5, \ldots$ $\tan\gamma_n/2 = h/\gamma_n$ and for $n = 2, 4, 6, \ldots$ $\tan\gamma_n/2 = -\gamma_n/h$.

Hence for n odd, $B_n = \gamma_n^2 + h^2$ and $C_n = 0$. For n even, $B_n = 0$ and $C_n = \gamma_n^2 + h^2$.

Defining $\beta_m = \gamma_{2m-1}$ and $\delta_m = \gamma_{2m}$ for $m = 1, 2, 3, \ldots$ and replacing $\bar{\varsigma}$ by ς and $\bar{\varsigma}'$ by ς' we obtain

$$T = \frac{\Omega\,\mathrm{e}^{-U^2/4\tau}}{2\pi\tau}\sum_{m=1}^{\infty}\left\{\frac{\cos\beta_m\varsigma\cos\beta_m\varsigma'}{1+2h/(\beta_m^2+h^2)}\,\mathrm{e}^{-(\beta_m w/L)^2\tau} + \frac{\sin\delta_m\varsigma\sin\delta_m\varsigma'}{1+2h/(\delta_m^2+h^2)}\,\mathrm{e}^{-(\delta_m w/L)^2\tau}\right\}. \quad \text{(A.3)}$$

Equation (A.3) with

$$\tan\beta_m/2 = h/\beta_m \quad \text{(A.4)}$$

and $\tan\delta_m/2 = -\delta_m/h$ satisfies the boundary conditions: $[hT \pm \partial T/\partial\zeta]_{\zeta=\pm1/2} = 0$.

The rate of heat generation per unit volume due to a Gaussian beam is $\alpha_a I(u', \zeta', \tau')$ where $I(u', \zeta', \tau') = I_p \exp\{-2u'^2 - \alpha L(\zeta' + 1/2)\}$, I_p = peak irradiance, α = extinction coefficient and α_a = linear absorption coefficient. The power absorbed in a single pass

$$\rho c w^2 L\Omega/t_K = P_{abs} = 2\pi\alpha_a w^2 L\int_0^{\infty}\mathrm{d}u'\,u'\int_{-1/2}^{1/2}\mathrm{d}\varsigma'\,I(u',\varsigma') = \frac{\pi w^2 I_p\alpha_a}{2\alpha}(1-\mathrm{e}^{-\alpha L}). \quad \text{(A.5)}$$

Hence, if $\alpha L \ll 1$, $I_p = 2P_{abs}/\pi\alpha_a L w^2$. For a thin sample, we replace $\alpha_a I(u', \zeta', \tau')$ by its axial average, $\alpha_a I_p(1-\mathrm{e}^{-\alpha L})[\exp(-2u'^2)]/\alpha L = (2P_{abs}/\pi L w^2)\exp(-2u'^2)$. The temperature due to an instantaneous cylindrical Gaussian source of this strength at time $\tau' = 0$ is therefore

$$T = \frac{2P_{abs}t_K}{\pi\rho c}\int_0^{\infty}\mathrm{d}u'\,u'\int_0^{2\pi}\mathrm{d}\theta'\int_{-1/2}^{1/2}\mathrm{d}\varsigma'\,G(u,\varsigma,\theta,\tau;u',\varsigma',\theta',\tau'=0)\exp(-2u'^2) \quad \text{(A.6)}$$

where

$$G = \frac{\mathrm{e}^{-U^2/4\tau}}{2\pi\tau L w^2}\sum_{m=1}^{\infty}\left\{\frac{\cos\beta_m\varsigma\cos\beta_m\varsigma'}{1+2h/(\beta_m^2+h^2)}\,\mathrm{e}^{-(\beta_m w/L)^2\tau} + \frac{\sin\delta_m\varsigma\sin\delta_m\varsigma'}{1+2h/(\delta_m^2+h^2)}\,\mathrm{e}^{-(\delta_m w/L)^2\tau}\right\}. \quad \text{(A.7)}$$

After carrying out the integrations with respect to ζ' and θ', using $\int_0^{2\pi}\mathrm{d}\theta'\exp[-2uu'\cos(\theta-\theta')/4\tau] = 2\pi I_0(uu'/2\tau)$ where I_0 is a modified Bessel function of the first kind of order 0, equation (A.6) becomes

$$T = \frac{4P_{abs}t_K\,\mathrm{e}^{-u^2/4\tau}}{\pi\rho c\tau w^2 L}\int_0^{\infty}\mathrm{d}u'\,u'\exp\left\{-u'^2\left(2+\frac{1}{4\tau}\right)\right\}I_0\left(\frac{uu'}{2\tau}\right) \times\sum_{m=1}^{\infty}\frac{\cos\beta_m\varsigma\sin\beta_m/2}{\beta_m\{1+2h/(\beta_m^2+h^2)\}}\,\mathrm{e}^{-(\beta_m w/L)^2\tau}. \quad \text{(A.8)}$$

Now

$$\int_0^{\infty}\mathrm{d}u'\,u'\exp(-a^2u'^2)I_0(bu') = \frac{1}{2a^2}\exp(b^2/4a^2) \quad \text{(A.9)}$$

(Prudnikov *et al* 1986).

Hence, on reversing the integration and summation in equation (A.8) and re-instating the notation $\bar{\varsigma}$, we obtain

$$T = \frac{8P_{abs}t_K}{\rho c\pi L w^2}\sum_{m=1}^{\infty}\frac{\cos\beta_m\bar{\varsigma}\sin\beta_m/2}{\beta_m\{1+2h/(\beta_m^2+h^2)\}}\frac{\exp\{-2u^2/(1+8\tau)-(\beta_m w/L)^2\tau\}}{1+8\tau}.$$

The Green function for an instantaneous source at time τ' is obtained by substituting $\tau - \tau'$ for τ in (A.7). Hence the temperature at time τ due to a source of constant strength switched on at time $\tau' = 0$ is

$$T = \frac{8P_{abs}}{\pi LK}\sum_{m=1}^{\infty}\frac{\cos\beta_m\bar{\varsigma}\sin\beta_m/2}{\beta_m\{1+2h/(\beta_m^2+h^2)\}}\int_0^{\tau}\frac{\mathrm{d}\tau'}{1+8\tau'}\exp\left(\frac{-2u^2}{1+8\tau'}-\frac{w^2\beta_m^2\tau'}{L^2}\right). \tag{A.10}$$

Setting $u = 0$ gives the time-dependent axial temperature due to the steady Gaussian source:

$$T = \frac{P_{abs}}{\pi LK}\sum_{m=1}^{\infty}\frac{\cos\beta_m\bar{\varsigma}\sin\beta_m/2}{\beta_m\{1+2h/(\beta_m^2+h^2)\}} \times\exp\left(\frac{w^2\beta_m^2}{8L^2}\right)\left[E_1\left\{\frac{w^2\beta_m^2}{8L^2}\right\}-E_1\left\{\frac{w^2\beta_m^2}{8L^2}(1+8\tau)\right\}\right] \tag{A.11}$$

and hence the steady-state axial temperature:

$$T = \frac{P_{abs}}{\pi LK}\sum_{m=1}^{\infty}\frac{\cos\beta_m\bar{\varsigma}\sin\beta_m/2}{\beta_m\{1+2h/(\beta_m^2+h^2)\}}\exp\left(\frac{w^2\beta_m^2}{8L^2}\right)E_1\left(\frac{w^2\beta_m^2}{8L^2}\right) \tag{A.12}$$

where $E_1(x)$ is the exponential integral function $\int_x^{\infty}\mathrm{d}t\,\mathrm{e}^{-t}/t$.

Appendix B. Solution of the slowly varying envelope equation with the Ein function

Substituting $E_F(u,\zeta) = E_0(u,\zeta)\exp[\{\mathrm{i}kn_0\zeta + \mathrm{i}kn_0S(u,\zeta) - \alpha\zeta/2\}L]$ into equation (2.10) and equating real and imaginary parts gives

$$(w/L)^2\partial E_0^2/\partial\varsigma + (\partial S/\partial u)\partial E_0^2/\partial u + E_0^2\{\partial^2 S/\partial u^2 + (\partial S/\partial u)/u\} = 0 \tag{B.1}$$

and

$$\left(\frac{w}{L}\right)^2\frac{\partial S}{\partial\varsigma}+\frac{1}{2}\left(\frac{\partial S}{\partial u}\right)^2 = \frac{1}{2k^2n_0^2L^2E_0}\left(\frac{\partial^2E_0}{\partial u^2}+\frac{1}{u}\frac{\partial E_0}{\partial u}\right)+\frac{w^2}{n_0L^2}\frac{\mathrm{d}n}{\mathrm{d}T}T(u). \tag{B.2}$$

Using the ansatz $S(u,\zeta) = \beta(\zeta)\mathrm{Ein}(2u^2) + \phi(\zeta)$, equation (B.1) becomes

$$(w/L)^2\partial E_0^2/\partial\varsigma + 2(\beta/u)(1-\mathrm{e}^{-2u^2})\partial E_0^2/\partial u + 8\beta\,\mathrm{e}^{-2u^2}E_0^2 = 0. \tag{B.3}$$

As in the approach based on the parabolic phase ansatz, we seek the appropriate functional form for E_0^2 by transforming to a new coordinate system in which E_0^2 takes a simple form. Changing the independent variables to $\eta = \eta(u,\zeta)$ and $\sigma = \sigma(u,\zeta)$ equation (B.3) gives

$$\left\{\left(\frac{w}{L}\right)^2\frac{\partial\eta}{\partial\varsigma}+\frac{2\beta}{u}(1-\mathrm{e}^{-2u^2})\frac{\partial\eta}{\partial u}\right\}\frac{\partial E_0^2}{\partial\eta}+\left\{\left(\frac{w}{L}\right)^2\frac{\partial\sigma}{\partial\varsigma}+\frac{2\beta}{u}(1-\mathrm{e}^{-2u^2})\frac{\partial\sigma}{\partial u}\right\}\frac{\partial E_0^2}{\partial\sigma} +8\beta\,\mathrm{e}^{-2u^2}E_0^2 = 0. \tag{B.4}$$

Setting $(w/L)^2\partial\eta/\partial\varsigma + (2\beta/u)(1-\mathrm{e}^{-2u^2})\partial\eta/\partial u = 0$ with $\eta = Z_\eta(\varsigma)U_\eta(u)$ gives

$$-(w/L)^2Z_\eta'/\beta Z_\eta = 2(1-\mathrm{e}^{-2u^2})U_\eta'/uU_\eta = \text{constant}.$$

Hence an appropriate choice for η is $\eta = \mathrm{e}^{g(\varsigma)}(\mathrm{e}^{2u^2}-1)$ with $g(\varsigma) = -8(L/w)^2\int\beta(\varsigma)\,\mathrm{d}\zeta$.

We now transform equation (B.4) into

$$\sigma\,\partial E_0^2/\partial\sigma + E_0^2 = \partial(\sigma E_0^2)/\partial\sigma = 0 \tag{B.5}$$

by choosing σ such that

$$(w/L)^2\partial\sigma/\partial\varsigma + (2\beta/u)(1-\mathrm{e}^{-2u^2})\partial\sigma/\partial u = 8\beta\,\mathrm{e}^{-2u^2}\sigma$$

with $\sigma = Z_\sigma(\varsigma)U_\sigma(u)$.

Hence

$$-(w/L)^2 Z'_\sigma/\beta Z_\sigma = 2(1-\mathrm{e}^{-2u^2})U'_\sigma/uU_\sigma - 8\,\mathrm{e}^{-2u^2} = \text{constant}.$$

So we choose

$$\sigma = \mathrm{e}^{g(\varsigma)}(1-\mathrm{e}^{-2u^2})^2\,\mathrm{e}^{2u^2}.$$

Then equation (B.5) gives $E_0^2 = Y(\eta)/\sigma$ where Y is an arbitrary function of η.

To satisfy the boundary condition $E_0^2 = I_p\,\mathrm{e}^{-2u^2}$ we must have

$$E_0(u,\varsigma) = E_p \exp\tfrac{1}{2}\{-g(\varsigma) - 2u^2\}/[1 + \{\mathrm{e}^{-g(\varsigma)} - 1\}\exp(-2u^2)].$$

Substituting for E_0^2 in equation (B.2) we obtain an equation for $g(\zeta)$:

$$\beta'\mathrm{Ein}(2x) + \phi' + \frac{2L^2\beta^2}{w^2u^2}(1-\mathrm{e}^{-2x})^2 = \frac{2\{(x+1)p^2\,\mathrm{e}^{-2x} + (x-1)\,\mathrm{e}^{2x} - 6px\}}{k^2n_0^2w^2(\mathrm{e}^x - p\,\mathrm{e}^{-x})^2} + \frac{1}{n_0}\frac{\mathrm{d}n}{\mathrm{d}T}T(u) \tag{B.6}$$

where $x \equiv u^2$ and $p \equiv \mathrm{e}^{-g} - 1$.

Setting $u = 0$ in equation (B.6) we obtain an equation for $\phi'(\zeta)$:

$$\phi'(\varsigma) = \frac{2(p-1)}{k^2n_0^2w^2(p+1)} + \frac{1}{n_0}\frac{\mathrm{d}n}{\mathrm{d}T}T(0)$$

which gives $\phi'(\zeta)$ once $g(\zeta)$ is known.

Substituting for $\phi'(\zeta)$ in equation (B.6) gives

$$\beta'\mathrm{Ein}(2x) + \frac{2L^2\beta^2}{w^2u^2}(1-\mathrm{e}^{-2x})^2 = \frac{2\{(x+1)p^2\,\mathrm{e}^{-2x} + (x-1)\,\mathrm{e}^{2x} - 6px\}}{k^2n_0^2w^2(\mathrm{e}^x - p\,\mathrm{e}^{-x})^2} - \frac{2(p-1)}{k^2n_0^2w^2(p+1)} - \frac{C}{n_0}\frac{\mathrm{d}n}{\mathrm{d}T}\mathrm{Ein}(2x)$$

where $C = A_sP/4\pi LK$. To first order in x (equating coefficients of u^2) we obtain

$$\beta' = \frac{p^2 - 10p + 1)}{k^2n_0^2w^2(p+1)^2} - \frac{C}{n_0}\frac{\mathrm{d}n}{\mathrm{d}T}$$

$$\text{i.e. } -\frac{w^2}{8L^2}g'' = \frac{1 - 12\,\mathrm{e}^g + 12\,\mathrm{e}^{2g}}{k^2n_0^2w^2} - \frac{C}{n_0}\frac{\mathrm{d}n}{\mathrm{d}T}$$

$$\therefore \qquad \frac{\mathrm{d}(\frac{1}{2}g'^2)}{\mathrm{d}g} = 8L^2\{C(\mathrm{d}n/\mathrm{d}T)/n_0 - (1 - 12\,\mathrm{e}^g + 12\,\mathrm{e}^{2g})/k^2n_0^2w^2\}/w^2.$$

Now $g(0) = 0 = g'(0)$ so

$$\frac{1}{2}g'^2 = 8L^2Cg(\mathrm{d}n/\mathrm{d}T)/n_0w^2 - 8L^2(g - 12\,\mathrm{e}^g + 6\,\mathrm{e}^{2g} + 6)/k^2n_0^2w^4.$$

The solution of this equation is discussed in section 5.

Acknowledgments

We thank Professor H Schmid and Dr Z-G Ye for providing PMN samples and Professor K S No and Professor Wu for providing PLZT samples. We acknowledge the assistance of Dr Olga Gredeskoul in preparing the glossary of symbols. Work at Cambridge was supported by a grant from the EPSRC and the Leverhulme Foundation.

References

Abraham N B and Firth W J 1990 *J. Opt. Soc. Am.* B **7** 951

Abramowitz M and Stegun I A (eds) 1964 *Handbook of Mathematical Functions* (Washington: US Government Printing Office) sections 9.6.12, 9.6.13; also p 228

Akhmanov S A, Krindach D P, Migulin A V, Sukhorukov A P and Kohkhlov R V 1968a *J. Quantum Electron.* **4** 568

Akhmanov S A, Krindach D P, Sukhorukov A P and Kohkhlov R V 1967 *Pis. Zh. Eksp. Teor. Fiz.* **6** 509 (Engl. Transl. *JETP Lett.* **6** 38)

Akhmanov S A, Sukhorukov A P and Khokhlov R V 1968b *Sov. Phys.–Usp.* **10** 609

Altshuler G A, Ermolyayev V S, Hramov V Yu, Zauls V and Liberts G 1986 *Ferroelectrics* **69** 67

Bannerjee P P, Yu H L, Gregory D A, Kuchtarev N and Caulfield H J 1995 *Opt. Lett.* **20** 11

Beale P D, Chen T, Sheih S-J and Scott J F 1991 *Ferroelectrics* **123** 1

Becker P J and Gehring G A 1975 *Solid State Commun.* **16** 795

Benkert C and Anderson D Z 1991 *Phys. Rev.* A **44** 4633

Bjorkholm J E, Smith P E and Tomlinson W J 1982 *IEEE J. Quantum Electron.* **18** 2016

Borenstein M and Lamb E 1972 *Phys. Rev.* A **5** 1298

Burkhart G H and Rice R R 1977 *J. Appl. Phys.* **48** 4817

Carslaw H S and Jaeger J C 1959 *Conduction of Heat in Solids* 2nd edn (Oxford: Clarendon)

Chen T, Sheih S-J and Scott J F 1991a *Phys. Rev.* B **43** 615

Chen T, Sheih S J, Scott J F and Bhalla A 1992 *Appl. Phys. Lett.* **60** 332

Chen T, Sheih S-J, Scott J F and Chen H 1991b *Ferroelectrics* **120** 115 report oscillation in both $Sr_xBa_{1-x}Nb_2O_6$ and $Ba_2NaNb_5O_{15}$, in addition to the PMN and PLZT results elsewhere.

Chen T and Scott J F 1993a *Ferroelectrics* **143** 149

——1993b *Integ. Ferroelectr.* **3** 69

Chen T, Scott J F and Phillipson P E 1994 *Integ. Ferroelectr.* **5** 1

Chen Z, Shibata M, Adachi M and Kawabata A 1995 *Japan. J. Appl. Phys.* **34** 5396

Cheung M-M, Durbin S D and Shen Y R 1983 *Opt. Lett.* **8** 39

Corduneanu C 1991 *Integral Equations and Applications* (Cambridge: Cambridge University Press) p 19

Courtens E and Gammon R W 1981 *Phys. Rev.* B **24** 3890

Dagenais M, Surkis A, Sharfin W F and Winful H G 1985 *IEEE J. Quantum Electron.* **21** 1458

Fatuzzo E 1964 *Proc. Phys. Soc.* **84** 709

Felber F S and Marburger J H 1976 *Appl. Phys. Lett.* **28** 731

Firth W J 1987 *Phys. Lett.* A **8** 375

——1990 *J. Mod. Opt.* **37** 151

Firth W J, Galbraith L and Wright E M 1985 *J. Opt. Soc. Am.* B **2** 1005

Gagnon L 1990 *J. Opt. Soc. Am.* B **7** 1098

Garmire E 1989 *IEEE J. Quantum Electron.* **25** 289

Gehring G A 1976 *J. Phys.: Condens. Matter* **10** 531

Ghatak A K and Thyagarajan K 1978 *Contemporary Optics* (New York: Plenum) ch 9

Gibbs H 1985 *Optical Bistability* (Orlando, FL: Academic)

Gibbs H M, Hopf F A, Kaplan D L and Shoemaker R L 1981 *Phys. Rev. Lett.* **46** 474

Goldstone J A and Garmire E 1981 *IEEE J. Quantum Electron.* **3** 366

Gordon J P, Leite R C, Moore R S, Porto S P S and Whinnery J R 1965 *J. Appl. Phys.* **36** 3

Grindrod P 1991 *Patterns and Waves: the Theory and Applications of Reaction–Diffusion Equations* (Oxford: Clarendon)

Grohs J, Mueller M, Schmidt A, Uhrig A, Klingshirn C and Bertelt H 1990 *Opt. Commun.* **78** 77

Grynberg G 1988 *Opt. Commun.* **66** 321

Gutowski J, Hollandt J and Broser I 1989 *Z. Phys.* B **53** 547

Hackbush W 1995 *Integral Equations* (Basel: Birkhauser) p 25

Haddad I, Kretzschmar M, Rossmann H and Henneberger F 1986 *Phys. Status Solidi* b **138** 235

Hajto J and Janossy I 1983 *Phil. Mag.* B **47** 347

Harley R T and Macfarlane R M 1975 *J. Phys.: Condens. Matter* **8** L451

Harrison R G, Firth W J and Al-Saidi I A 1984 *Phys. Rev. Lett.* **53** 258

Harrison R G, Firth W J, Emshary C A and Al-Saidi I A 1983 *Phys. Rev. Lett.* **51** 562

Honda T 1993 *Opt. Lett.* **18** 598

——1995 *Opt. Lett.* **20** 851

Ikeda H 1979 *Opt. Commun.* **30** 257

Ikeda H, Daido H and Akimoto O 1980 *Phys. Rev. Lett.* **45** 709

Jewell J L, Gibbs H M, Tarng S S, Gossard C and Weigmann W 1982 *Appl. Phys. Lett.* **40** 291

Jaeger D, Forsmann F and Wedding B 1985 *IEEE J. Quantum Electron.* **27** 1453
Kerner B S and Osipov V V 1994 *Autosolitons: a New Approach to Problems of Self-Organization and Turbulence* (Dordrecht: Kluwer)
Khoo I C, Yan P Y, Liu T H, Shepard S and Hou J Y 1984 *Phys. Rev.* A **29** 2756
Korshunov O Yu, Markovin P A and Pisarev R V 1992 *Ferroelectr. Lett.* **13** 137
Kretzschmar M, Henneberger F, Rossmann H and Haddad I 1987 *Phys. Status Solidi* b **143** K71
Krumins A, Anspoks A, Odoulov S G, Seglins J and Vaivods P 1988 *Ferroelectrics* **80** 277
Krumins A *et al* 1994 *Proc. 5th Russian–Japan. Symp. on Ferroelectrics* (Moscow: Akademiya Nauki) p 244
Krumins A, Chen Z, Ishii M, Shiosaki T and Kawabata A 1995 *Ferroelectrics* **169** 259
Krumins A, Chen Z, Shibata M and Belov A A 1996 *Ferroelectrics* **183** 171
Kurtz S K, Kozikowski S D and Wolfram L J 1987 *Electrooptic and Photorefractive Materials* ed P Gunter (Berlin: Springer) p 110
Lambsdorff M, Doernfield C and Klingshirn C 1986 *Z. Phys.* B **64** 409
Landolt–Börnstein New Series 1961 *Group III* ed K H Hellwege (Berlin: Springer) p 101
Lotka A J 1925 *Elements of Physical Biology* (Baltimore: Baltimore)
Macdonald R and Eichler H J 1992 *Opt. Commun.* **89** 289
Mante A J H and Volger J 1967 *Phys. Lett.* A **24** 139
Marburger J H and Felber F S 1978 *Phys. Rev.* A **17** 335
May R M and Leonard W J 1975 *SIAM J. Appl. Math.* **29** 243
Miller D A B 1981 *IEEE J. Quantum Electron.* **17** 306
Miller D A B, Smith S D and Seaton C T 1981 *IEEE J. Quantum Electron.* **17** 317
——1984 *J. Opt. Soc. Am.* B **1** 857
Moloney J V and Gibbs H M 1982 *Phys. Rev. Lett.* **48** 1607
Nakatsuka N, Asaka S, Itoh H, Ikeda K and Matsuoka M 1983 *Phys. Rev. Lett.* **50** 109
Nettleton R E 1970 *Ferroelectrics* **1** 87
O'Sullivan R A, Zheng X, Scott J F, Ye Z G and Schmid H 1995 *Integ. Ferroelectr.* **9** 215
——1996a *Ferroelectrics* **186** 17
O'Sullivan R A, McGregor K W, Cianci S, Sacca R, Wilksch P A and Scott J F 1996b *Japan. J. Appl. Phys.* **35** 5203
Ozolinsh M, Hanstorp D and Lagerwall S T 1997 *Ferroelectrics* **201** 295
Prudnikov A P, Brychkov Yu A and Marichev O I 1986 *Integrals and Series* vol 2 (New York: Gordon and Breach) p 306
Reinisch R and Vitrant G 1990 *J. Appl. Phys.* **67** 11
Rozanov N N 1981 *Zh. Eksp. Teor. Fiz.* **80** 96 (Engl. Transl. 1981 *Sov. Phys.–JETP* **53** 47)
Rozanov N N and Semenov 1980 *Opt. Spectrosc. (USSR)* **48** 1
Sargent M, Scully M O and Lamb W E 1974 *Laser Physics* (New York: Addison-Wesley) pp 45–51, 120–127
Scalora M and Haus J W 1989 *J. Opt. Soc. Am.* B **6** 1714
Scott J F 1975 *Opt. Commun.* **15** 343
——1986 Phase transitions in nonequilibrium systems: dye lasers and lasers with saturable absorbers *Frontiers of Nonequilibrium Statistical Physics* ed G T Moore and M O Scully (New York: Plenum, NATO Series B, Vol. 135) pp 465–72
Scott J F and Chen T 1992 *Integ. Ferroelectr.* **1** 71
Scott J F, Chen T and Sheih S-J 1991 *Ferroelectrics* **117** 21
Scott J F and O'Sullivan R A 1996 *Nature* **382** 305
Scott J F, O'Sullivan R A and Reich M H 1996 *Physica* A **223** 655
Scott J F, Sargeant M and Cantrell J D 1975 *Opt. Commun.* **15** 13
Scott J F and Sheih S-J 1990 *J. Phys.: Condens. Matter* **2** L8553
Scott J F *et al* 1990 *Phys. Rev.* B **41** 9330
Seglins J, Krumins A, Anspoks A, Odoulov S G and Vaivods P 1988 *Ferroelectrics* **80** 277
Seglins J A, Krumins A, Ozols A and Odoulov S G 1987 *Ferroelectrics* **75** 317
Sheih S-J, Chen T, Beale P D and Scott J F 1991 *Ferroelectrics* **123** 1
Sievers A J 1963 *Bull. Am. Phys. Soc.* **8** 208
Smith S D, Matthew J G H, Taghizadeh M R, Walker A C and Wherrett B S 1984 *Opt. Commun.* **51** 357
Steverding B 1976 *J. Appl. Phys.* **47** 1467
Tonelli L 1928 *Math. Ann.* **99** 183. See also Corduneanu 1991, p 98
Vitrant G, Haeltermann M and Reinisch R 1990a *J. Opt. Soc.* B **7** 1319
——1990b *J. Appl. Phys.* **67** 6671
Volterra V 1926 *Memoirs of the Academia dei Lincei* (Rome)
——1931 *Leçns sur la Théorie Mathematique de la Lutte pour la Vie* (Paris: Gauthier-Villars)

Wagner W G, Haus H A and Marburger J H 1968 *Phys. Rev.* **175** 256
Watson G N 1966 *A Treatise on the Theory of Bessel Functions* 2nd edn (Cambridge: Cambridge University Press) p 395
Weaire D and al-Hourani M 1990 *J. Opt. Soc. Am.* B **7** 1066
Weaire D and Kermode J P 1986 *J. Opt. Soc. Am.* B **3** 1706
Weaire D, Kermode J P and Dwyer V M 1985 *Opt. Commun.* **55** 223
——1986 *J. Opt. Soc. Am.* B **3** 1706
Wegener M and Klingshirn C 1987 *Phys. Rev.* A **35** 1740
Wherrett B S 1984 *IEEE J. Quantum Electron.* **20** 646
Whinnery J R, Miller D T and Dabby R W 1967 *IEEE J. Quantum. Electron.* **3** 382
Wood I G, David W I F, Glazer A M and Welber B 1980 *J. Appl. Crystallogr.* **13** 224
Wood I G and Glazer A M 1980 *J. Appl. Crystallogr.* **13** 217
Wright E M, Firth W J and Galbraith I 1985 *J. Opt. Soc. Am.* B **2** 383
Yamada T, Iwasaki H and Niizeki N 1970 *J. Appl. Phys.* **41** 4141
Yokoyama H 1989 *IEEE J. Quantum Electron.* **25** 1190
Yoshida I 1960 *J. Phys. Soc. Japan* **15** 2211
Zheng X, O'Sullivan R A and Scott J F 1995 *Integ. Ferroelectr.* **9** 225